Toward improvement of microphysical processes within the melting layer

Yasushi Fujiyoshi
Inst. Low Temp. Sci., Hokkaido University, Sapporo, Japan

1. Introduction

The melting layer is a frontier left in precipitation physics.

The melting layer plays important roles in the formation of laminar structure of the atmosphere. The cooling due to melting particles can produce deep isothermal layers (Findeisen, 1940). This cooling can lead to a separation of the dynamics above and below the melting layer, and may be important on the large-, meso- and convective-scale phenomena (Atlas et al.,1969; Fabry et al., 1995).

In the melting layer, there appears a layer of enhanced radar-reflectivity, that is, "bright band". The bright band has been considered a source of error in precipitation estimates using spaceborne (TRMM) and ground-based radars. The effect of melting particles on electromagnetic wave propagation is also important in microwave communication.

Although the qualitative explanation of the reflectivity enhancement causing the bright band has been made early on (Ryde, 1946), there is still no consensus after 60 years on a quantitative assessment. Given the large number of factors that may influence the bright band shape, it is not surprising to have so many, often contradictory, explanations of the bright band phenomenon. Since our understanding of the microphysical processes within the melting layer is incomplete, additional efforts must be invested to quantify the mechanisms that satisfy modelers, cloud physicists, and radar meteorologists.

The main purpose of this paper is to present some new physical properties of melting particles observed by using a 2DVD (2-dimensional video disdrometer). This study will improve our understanding of physical processes within the melting layer.

2. Data

We used the two-dimensional video disdrometer (2DVD) (Schönhuber et al., 1997; Kruger and Krajewski, 2002) to measure size, shape, axis ratio (oblateness), canting angle, and velocity of precipitation particles. The 2DVD data were collected over a 6-year period from 2004 to 2008 at Sapporo, and over a 5-year period from 2004 to 2008 at Kanazawa.

3. Melting snowflakes

During melting, the fall velocity of melting snowflakes increases as water accumulation increases their bulk density. Based on their laboratory experiments, Mitra et al. (1990) showed that the fall velocity depends on particle size and its melted fraction.

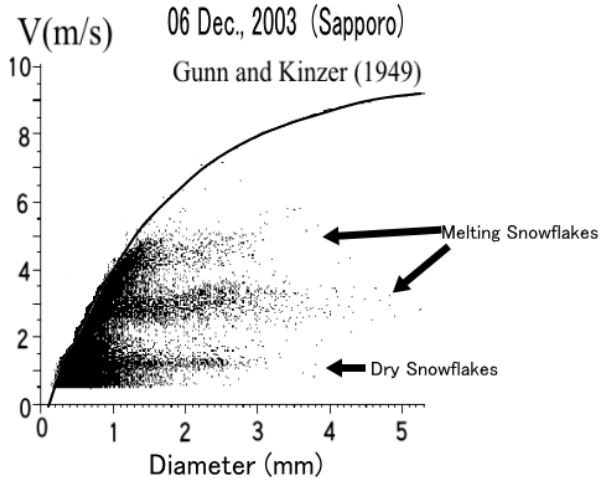

Fig. 1: Velocity-Diameter relationships of dry- and melting snowflakes measured by using a 2DVD at Sapporo on 6 Dec. of 2003.

Figure 1 clearly shows that melting snowflakes weakly depend on parameters such as shape, density, and size of particles as suggested by Matsuo and Sasyo (1981a,b). This result indicates that the most important parameter, that controls a fall velocity of a melting snowflake, is not the melted fraction, but total amount of melting water. This result also indicates that various sizes (and masses) of melting particles with the nearly the same fall velocity can exist together at the same level within the melting layer when these particles originate from snowflakes.

Since the shape of the melting snowflake decides the drag resistance and the ventilation coefficients, the microphysics of melting must be sensitive to the shape of the melting snowflakes. Examples of large melting snow particles observed at Kanazawa on 25 January 2005 are shown in Fig. 2. Large melting snowflakes (we call the typical shape of melting snowflakes the "Mickey Mouse" shape) fell between 00:24 and 00:34 JST, when the surface air temperature ranged from 7 to 8°C. Terminal fall velocities of dry snowflakes do not change with size because their drag resistance increases with size. On the other hand, the melting snowflakes can change their shape and drag resistance. Thus, the fall velocities of large melting snowflakes can be similar to those of raindrops (approximately 8 m

s^{-1}).

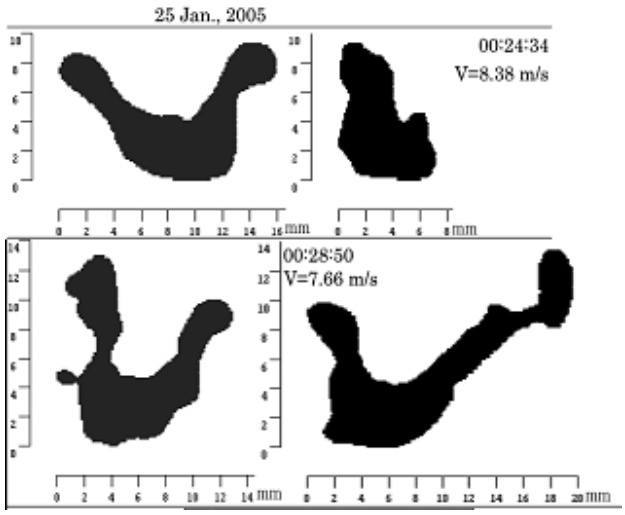

Fig.2: 2DVD images of large melting snow particles observed on 25 January 2005. The time of measurement and fall velocity are also shown.

4. Melting graupels

As shown in Fig. 3, fall velocities of dry graupels increase almost linearly with size (a dotted line). Since the density of melting graupels increases with decreasing size, the difference in fall velocities between dry- and melting graupels increases with decreasing size as shown in Fig.3. The Diameter-Velocity relationship of melting graupels in Fig. 3 can be explained by the theory presented by Matsuo and Sasyo (1981a,b).

Figure 4 shows examples of melting graupels. Aggregation of melting snowflakes occurs within the upper part of the melting layer (Barthazy et al., 1998). This 2DVD images clearly show that graupels can also aggregate with each other within the melting layer.

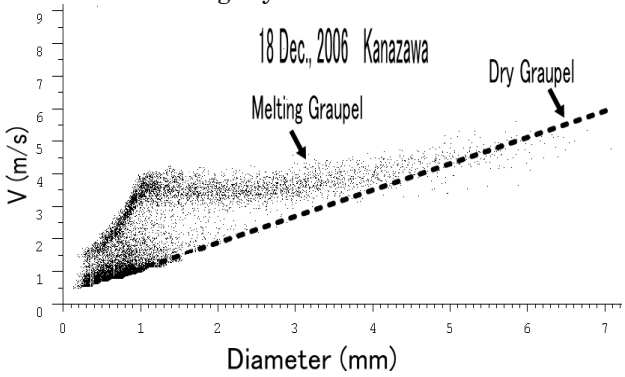

Fig. 3: Velocity-Diameter relationships of melting graupels measured by using a 2DVD at Kanazawa on 18 Dec. of 2006.

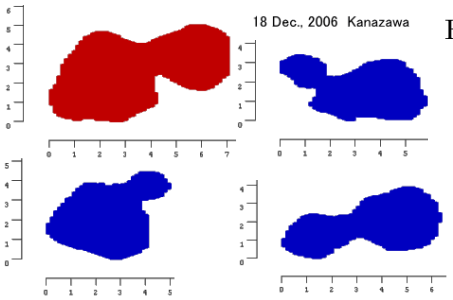

Fig.4: Images of aggregated melting graupels.

5. Concluding remarks

It is believed that observations presented here will help constrain bright band models. Outstanding problems include a more thorough evaluation of the contribution of shape or density effects, aggregation, and breakup of melting particles. We need realistic microphysical and scattering models to satisfy numerical modelers, cloud physicists and radar meteorologists.

References

Atlas, D., R. Tatehira, R. C. Srivastava, W. Marker, and R. E. Carbone,1969: Precipitation-induced mesoscale wind perturbations in the melting layer. *Quart. J. Roy. Meteor. Soc.,* **95,** 544–560.

Barthazy, E., W. Henrich, and A. Waldvogel, 1998: Size distribution of hydrometeors through the melting layer. *Atmos. Res.*, **47–48**, 193–208

Fabry, F., and I. Zawadzki, 1995: Long-term radar observations of the melting layer of precipitation and their interpretation. *J. Atmos. Sci.,* **52,** 838–851.

Findeisen, W, 1940: the formation of the O°C isothermal layer in fractocumulus and nimbostratus. *Meteologische Zeitshrift*, **57**, 49-54.

Kruger, A., and W. F. Krajewski, 2002: Two-dimensional video disdrometer: A description. *J. Atmos. Oceanic Technol.*, **19**, 602-617.

Matsuo, T. and Y. Sasyo, 1981a : Empirical formula for the melting rate of Snowflakes, *J. Meteor. Soc. Japan,* **59**, 1-9.

Matsuo, T. and Y. Sasyo, 1981b: Melting of snowflakes below freezing level in the atmosphere. *J. Meteor. Soc. Japan*, **59**, 26-32.

Mitra, S. K., O. Vohl, M. Ahr, and H. R. Pruppacher, 1990: A wind tunnel and theoretical study of the melting behavior of atmospheric ice particles. IV: Experiment and theory for snowflakes. *J. Atmos. Sci.,* **47,** 584–591.

Schönhuber, M., H. E. Urban, J. P. V. P. Baptista, W. L. Randeu, and W. Riedler, 1997: Weather radar vs. 2D-video-disdrometer data. Weather Radar Technology for Water Resources Management. B. Braga Jr. and O. Massambani, Eds., UNESCO Press.

Observations of solid precipitation particles using the Falling-Snow Observatory of Snow and Ice Research Center NIED in Nagaoka

Masaaki Ishizaka
Snow and Ice Research Center, NIED, Nagaoka, Japan

1. Introduction

The Falling-Snow Observatory of NIED (FSO) was established to observe solid precipitation particles precisely for understanding how they influence winter precipitation, deposited snow, and snow-related disasters. The FSO is consisted with two main facilities. One is operated for falling snow observation and the other for deposited snow observation. The former is a recording system of falling snows captured by a CCD camera. Images of them and positions in the captured area are translated into numerical data by image processing and stored in memories of a computer. The latter is a low-temperature room (–5°C) into which natural snows are falling through roof windows. We can catch falling particles in the room and examine them carefully under a microscope after taking photographs.

Comparing both observations in two facilities we could find that relations between particle size and fall speed, that were acquired from recording data of falling snows, well reflect types of solid precipitation. Therefore from the data of the automated recording system we could obtain continuous information about types of solid precipitation particles, i.e. graupel or aggregates in different riming stage, as well as other quantitative data, i.e. number of particles per unit volume and their size distribution, throughout winter season.

In this study we introduce how we recognize predominant types of precipitation particles in each snowfall event using the FSO and some observational results.

Fig. 1. Snapshot of the observation site.

2. Recording system of falling snow

For detecting the natural speed of falling hydrometeors, the measuring part of the system was placed in a space enclosed by double-net fences (Fig. 1). The configuration of recording system is shown in Fig. 2. Precipitation particles falling into the narrow space (0.2 m in width) under weak wind condition are illuminated by halogen lamps and photographed through the zoom lens of a CCD video camera set at a distance of 2 m. The shutter speed of the camera was set at 1/4000 second. At this high shutter speed, the displacement of particles due to falling motion was negligibly small. The size of captured image was 0.12 m (H) x 0.16 m (W) which corresponds to 240 pixels x 640 pixels.

Particles were recorded continuously for 1 second at every 5 seconds, and images were stored in an image processor (resolution: 240 x 640 dots, 256 levels). In the image processing, binarization of all captured images with an appropriate threshold level was carried out to detect precipitation particles. Then, for each detected particle, data concerning the position of the highest pixel, maximum horizontal width, lowest position, peripheral pixels and so on were calculated and stored in the computer's hard disk.

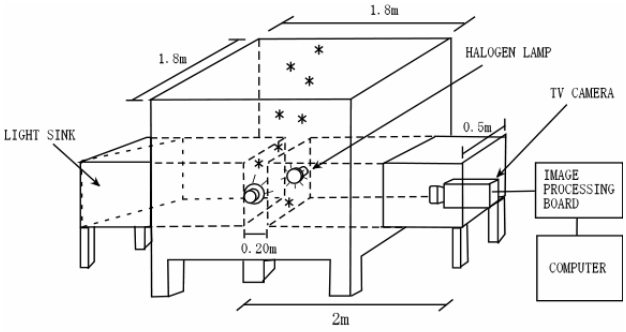

Fig. 2. Configuration of the automated recording system of falling snows..

3. Identification of types of solid particles

Operating the above automated recording system of particles, we carried out manned observations of fallen snows with a microscope during remarkable snowfall events in the low-temperature room (–5℃). We caught particles in the room and took microscopic photographs of particles. From these photographs, we could observe constituent crystals and extent of riming

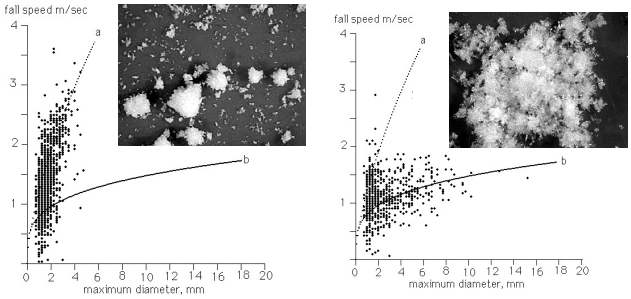

Fig. 3. Relationships between particle size and fall speed acquired from the recorded data and microscopic photos taken at same snowfall events.

of snowflakes, and types of graupel.

Figure 3 shows typical two cases of inter comparison between the manned observation and the recording data. Each spot in the graphs corresponds to size and fall speed of one particle measured by the automated recording system for about 10 minutes. Curves a and b in the graph are the best-fit curves of the cone-shaped graupel and the heavy rimed snowflake obtained by Locattelli and Hobbs, 1974. The microscopic photographs of predominant precipitation particles taken at the same period shown in the Figure. Left hand case and right hand one in the figure show that typical precipitation particles are cone-shaped graupel and heavily rimed snowflakes, respectively, and that the spots are distributed around corresponding best-fit curve. The same comparisons were carried out for cases of other types of solid precipitation particles and good agreements between size-speed relations and types of particles were found. These results suggested that the relationship between particle size and falling speed of snows acquired from numerical data well represented the types of precipitation particle and that we could obtain continuous information about types of solid hydrometeors from data of the recording system as well as quantitative data, i.e. numbers of particles of observed space and size distribution.

4. Observational resuls

We have worked the FSO every winter season from 2002-03 winter and could observe a few or several heavy snowfall events in a season. The observational results suggested that types of precipitation particles changed drastically according to precipitation system and they seemed to relate to 'snowfall modes' (Nakai,2005). The typical cases are shown in Fig.4. Snapshots of radar reflectivity of snowfall events (b) and (d) in Fig 4 show snowfall mode L-mode and S-mode respectively. In both cases the same mode lasted at least for a few hours. The size-speed graph a) and c) correspond to particles measured for about a hour during L-mode and S-mode period respectively. The observational results indicates that a predominant type of L-mode type precipitation was a graupel type and that of S-mode was a aggregates type. The same tendency was frequently found in our observations. Types of solid precipitation affect Z-R relation and estimation of precipitation amounts. so that to clarify the relation between types of particles and snowfall mode is important.

Moreover types of particles were also observed to affect density of deposited snow and accumulation rate of snow cover. Some kinds of snow crystals and large graupel were observed to form a weak layer in deposited snow which causes avalanche.

4. Future studies

Above mentioned size-speed relations are based on numbers of particles, but mass flux is more important. Now we are trying to translate the relation into that based on flux to clarify predominant types of solid precipitation during a target period. That might lead to more precise interpretation of relations between types of solid precipitations and snowfall mode, radar power return, precipitation process in a cloud, and other particle-type-related matters.

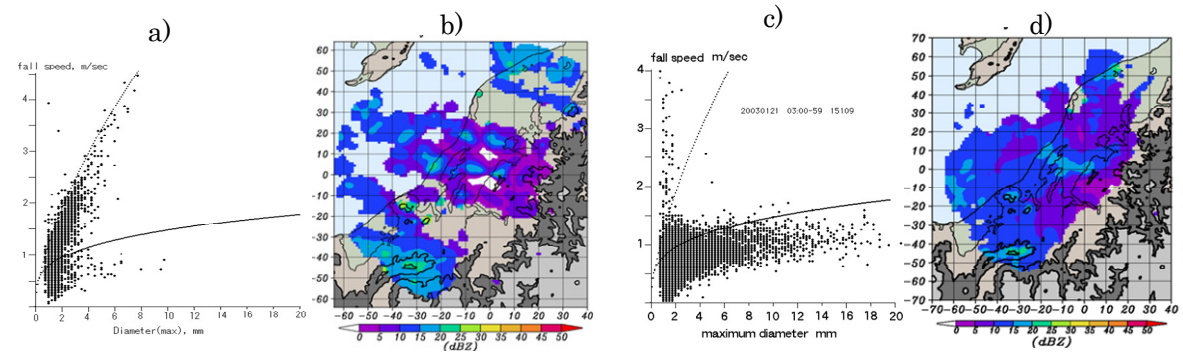

Fig. 4 Size and fall speed relations for particles fallen for 1 hour and snapshots of the radar echo patterns of the NIED radar at Nagaoka Institute, that express typical mode in the same periods.

A parcel model simulation of graupel and snowflake formation in convective snow clouds over the Sea of Japan

Ryohei Misumi†[1], Akihiro Hashimoto[2], Masataka Murakami[2], Naomi Kuba[3], Narihiro Orikasa[2], Atsushi Saito[2], Takuya Tajiri[2], Katsuya Yamashita[2], and Jen-Ping Chen[4]

[1]*National Research Institute for Earth Science and Disaster Prevention, Tsukuba, Japan*

[2]*Meteorological Research Institute, Tsukuba, Japan*

[3]*FRCGC/JAMSTEC, Yokohama, Japan*

[4]*National Taiwan University, Taipei, Taiwan*

1. Introduction

In winter monsoon seasons, convective snow clouds frequently develop over the Sea of Japan and bring great amount of snowfall along coastal regions. The main types of precipitating particles are graupels and snowflakes; the former causes local severe snowfall and the latter produces a long-term heavy snow. A modeling of the formation of graupels and snowflakes are important for snowfall forecasting as well as an improvement of general circulation models for predicting climate changes.

One typical procedure to simulate various types of snow particles is categorizing ice crystals into several classes such as cloud ice, snow, graupels and hails. A bulk cloud scheme calculates mixing ratio (and sometimes with number concentration) of each class, while spectral bin model predicts number density of particles every size bin. In such categorizing methods, however, particles having intermediate property between the classes are not taken into account, and a crystal in one class "jumps" into another class with its growth.

In order to simulate the formation of various types of precipitating particles, we need a microphysical model capable for calculating "continuous" transition between the classes. The model proposed by Chen and Lamb (1994) is very sophisticated, in which ice-crystal properties are represented in a multi-dimensional bin framework, including components of water mass, solute mass and aspect ratio. In the present study, we added "volume" as a new dimension to Chen and Lamb's model to simulate the formation of graupels and snowflakes more precisely. In this presentation we apply the modified Chen and Lamb's model to convective snow clouds over the Sea of Japan in a parcel model framework to understand the formation of solid precipitation.

2. Numerical simulation

The cloud model used in this study is a modified version of multi-dimensional bin model developed by Chen and Lamb (1994). Because the treatment of liquid water is the same as in the original model, we describe the calculation for ice particles here. We have six prognostic valuables in this model; total number, total heat, total water mass, total solute mass, total volume, and the sum of aspect ratio of particles. The calculation of chemical processes in the original model is not conducted here. Each prognostic valuable have four dimensions; water mass, solute mass, aspect ratio, and volume (Fig.1). The shape of ice crystals is assumed to be spheroid.

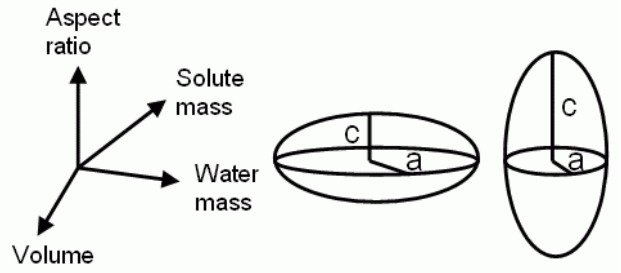

Fig.1. Shape of ice crystals and four components of dimensions.

Microphysical equations used here are essentially the same as in Chen and Lamb (1994), except for a slight modification in the aggregation efficiency. In order to avoid aggregation between graupels, we set aggregation efficiency as:

$$E_{agg} = \begin{cases} 1 - 0.99\,\rho_i / 0.2 & (\rho_i < 0.2\,gcm^{-3}) \\ 0.01 & (\rho_i \geq 0.2\,gcm^{-3}) \end{cases}$$

Here ρ_i is an averaged bulk density of colliding particles.

Numbers of bins for components of water mass, solute mass, aspect ratio and volume are 46, 45, 21 and 94, respectively. Because we pay our attention to the variation of bulk density, we set many bins for the volume. The calculation is conducted in a parcel model framework in which an air parcel rises adiabatically. Fallout of precipitating particles from the air parcel is not considered; thus our simulation is restricted to the development stage of convective snow clouds. We assumed a 1500 m-depth, parabolic updraft with maximum speed of 4 m/s. The beginning point of rising parcel is a cloud base at 900 hPa and -10℃. Calculation cases are listed in Table 1. In case *Control*, we use the "maritime surface"

distribution of Whitby (1978) for hygroscopic aerosols. Case *Urban* uses "urban average" aerosol distribution to test the sensitivity to the number of CCN. Homogeneous and immersion freezing of drops is off in case *No freeze* where we discuss the effects of drop freezing on the formation of precipitating particles. Case *Bulk* is the same calculation as *Control* except for using 1-moment bulk cloud scheme of Rutledge and Hobbs (1984). The numerical integrations were carried out until the parcels reach cloud top (20 minutes).

Table 1. Cases for calculation

Case	Physical process	Aerosols
Control	Full	Maritime surface
Urban	Full	Urban average
No freeze	No homogeneous/ immersion freezing	Maritime surface
Bulk	1-moment bulk model	

3. Results of the control case

The temperature of the parcel decreased almost linearly with height and reached -21.7℃ at the cloud top. This temperature is not out of the range of a typical convective snow clouds over the Sea of Japan (～-20℃). The CCN were activated just above the cloud base and formed cloud drops with 110 cm^{-3} in number density. Number of cloud drops slowly decreased with height due to their coalescence, and rapidly decreased at the cloud top by evaporation. Number concentration of ice particles, on the other hand, increased with height, and it reached 45 L^{-1} at the cloud top. This value is almost one order smaller than that of the video-sonde observation by Murakami et al. (1994) (300 L^{-1}). Particles with small aspect ratio (plates) prevailed below 1300 m, while spherical particles with high bulk density (graupels and densely rimed crystals) formed near the cloud top.

Size distributions of ice particles at the cloud top are shown in Fig.2. There are two peaks in the number concentration; one is at 200 μm and the other is 750 μm in the melted diameter. Takahashi (1993) found two separate modes in the graupel size in a convective snow clouds by his aircraft observation. However it is not clear whether the simulated two peaks correspond to his findings. Figure 3 is a visual illustration of the simulated ice particles "sampled" near the cloud top. Almost all particles show spherical shape with bulk density greater than 0.1 gcm^{-3}, which indicate the formation of graupels and densely rimed crystals.

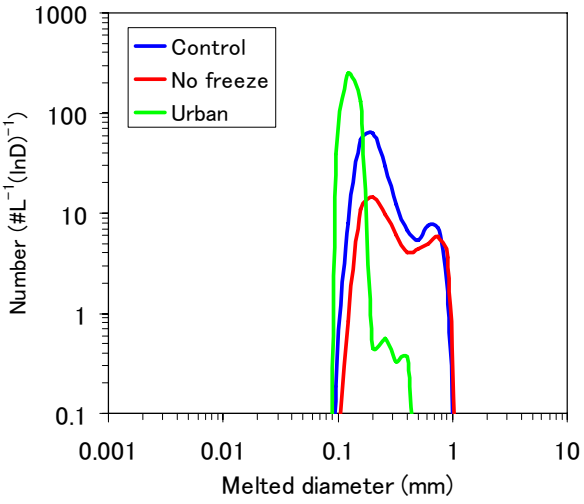

Fig.2. Size distribution of ice particles at the cloud top (20 minutes)

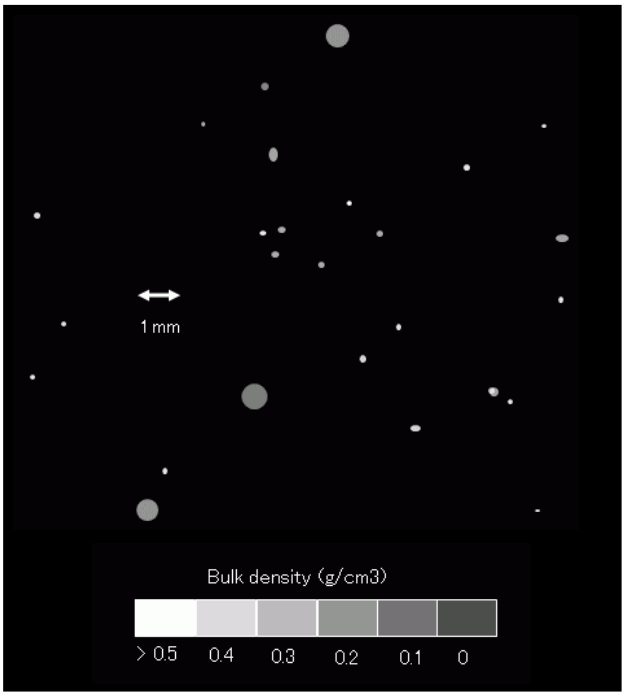

Fig. 3. Illustration of ice particles "sampled" at the cloud top in case *Control*. Oblate and prolate spheroids are drawn as horizontally long and vertically long ellipses, respectively. The gray scale indicates bulk density.

4. Results of sensitivity tests

In case *Urban,* in which urban average distribution of aerosols were given, number concentration of cloud drops exceeded 5000 cm^{-3} and more than 150 L^{-1} of ice crystals were formed. The excess amount of ice particles restricted their growth and the number of particles larger than 200 μm was much smaller than that in *Control* (Fig.2). In case *No freeze*, the number of ice particles with diameter around 200 μm decreased,

while that around 750 μm was not so changed. This suggests that plate-like crystals originating from deposition or condensation-freezing nucleation act as embryo of large particles formed near the cloud top. Case *Bulk* successfully simulated the total mixing ratio of ice particles and the lack of small crystals (cloud ice) at the cloud top. However "snow" did not exist in the bulk model, although ice particles with bulk density smaller than 0.2 gcm^{-3} existed in case *Control*.

5. Summary

Using a modified version of the multi-dimensional bin model of Chen and Lamb (1994), we conducted a parcel model simulation of convective snow clouds over the Sea of Japan. The results are summarized as follows:

1) Both deposition/condensation-freezing nucleation and homogeneous/immersion freezing of drops were effective for ice initiation of convective snow clouds over the Sea of Japan. However the simulated ice number concentration was almost one order smaller than that of observations.
2) At the cloud top there were two peaks in number concentration of ice particles. Sensitivity tests suggest that the embryos of the smaller peak consisted of frozen-drops, while those of the larger peaks were plate-like crystals originating from ice nuclei.
3) Excess amount of CCN increased number concentration of ice but restricted their growth.
4) The 1-moment bulk cloud scheme by Rutledge and Hobbs (1984) showed almost consistent results to our model, except for the absence of "snow".

Now the cloud model shown in this study is being installed in the Japan Meteorological Agency Non-Hydrostatic Model (JMA-NHM) under the Japanese Cloud Seeding Experiment for Precipitation Augmentation (JCSEPA). The model is also being used for improvement of the snow forecasting model in the Snow and Ice Research Group, NIED, in the Research Project for Developing a Snow Disaster Forecasting System and Snow Hazard Maps.

References

Chen, J.-P. and D. Lamb, 1994: Simulation of cloud microphysical and chemical processes using a multicomponent framework. Part I: Description of the microphysical model. J. Atmos. Sci., 51, 2613-2630.

Murakami, M., T. Matsuo, H. Mizuno and Y. Yamada, 1994: Mesoscale and microscale structures of snow clouds over the Sea of Japan. Part I: Evolution of microphysical structures in short-lived convective snow clouds. J. Meteor. Soc. Japan, 72, 671-694.

Rutledge S. A. and P. V. Hobbs, 1984: The mesoscale and microscale structure and organization of clouds and precipitation in midlatitude cyclones. XII: A diagnostic modeling study of precipitation development in narrow cold-frontal rainbands. J. Atmos. Sci., 41, 2949-2972.

Takahashi, T., 1993: High ice crystal production in winter cumuli over the Japan Sea. Geophys. Res. Lett., 20, 451-454.

The effect of bacteria and mineral dust as ice nuclei on the formation of snow and graupel simulated with a regional model

Jen-Ping Chen and Anupam Hazra
Department of Atmospheric Sciences, National Taiwan University

Abstract

for the 2009 International Workshop on radar and modeling studies of snowfall: Precise observation and modeling of solid precipitation

Atmospheric dust particles are one of the most uncertain factors contributing to the effects of aerosols on global climate processes. They may affect clouds directly through their activation into cloud drops or heterogeneous nucleation into ice crystals, thus are of great importance in precipitation development particularly in the mid-to-high latitudes. Laboratory experiments of ice nucleation by clay minerals have been shown by different nucleation modes, including deposition nucleation, condensation-freezing and immersion freezing. Mineral dust particles are commonly found to attach with hygroscopic material, such as sulfate, which may affect their nucleating capability in the freezing modes. Such influences by solute have also been studied experimentally for hematite, corundum and kaolinite particles. These data on ice formation in pure water and in aqueous solution with dust core are crucial for the understanding of natural influence on cloud and precipitation formation. Similar influences can also be exerted by bacteria which are also commonly present in the atmosphere but with higher ice nucleating capability than mineral dust.

In this study, the rates of ice nucleation by mineral dust particles and bacteria measured in the laboratory are theoretically analyzed and parameterized into formulations that may include the solute effect. The parameterization formulas are incorporated into a non-hydrostatic mesoscale cloud model modified with a two-moment warm-cloud parameterization and coupled with a two-moment ice-phase scheme, which explicitly predicts the masses and numbers of cloud particles, to examine the importance of ice processes on precipitation formation. Sensitivity simulations were performed for the role of mineral dust in their ice nucleation by (a) deposition nucleation, (b) immersion freezing in pure drops, and (c) immersion freezing in ammonium-sulfate solution drops. Additional comparison was done with bacteria nucleation in the immersion freezing mode. Various microphysical production terms such as the initiation, deposition growth, riming, melting for cloud ice, snow and graupel have been analyzed to examine the detailed mechanisms through which these ice nuclei affect precipitation formation.

Due to contact angle differences, nucleation by mineral dust by the deposition mode may occur at warmer temperatures than by the immersion freezing mode. Therefore, ice initialization in convective clouds may occur earlier at the lower levels by the deposition nucleation, without which ice formation can occur only when the convection can reach the upper levels where immersion freezing may proceed. Temperatures for immersion freezing are even lower when the solute effect comes into play. However, earlier or stronger nucleation not necessarily lead to more precipitation because up to a certain point the high concentration of ice particles will limit their growth in size due to competition for the available water. In the cases that

we analyzed using typical mineral dust concentration, nucleation in the deposition mode produced a high concentration of cloud ice which grow very fast into snow by vapor deposition. Yet, the snow that formed can grow very little by deposition, as the remaining water vapor is very little. Furthermore, because of the reduction of fall speed due to size limitation, the snow particles are refrained from falling to the lower levels that may provide more liquid water for the Bergeron-Findeisen conversion or riming growth. With only the freezing nucleation, snow and graupel particles are fewer but bigger, and they actually produced more rain when falling to the lower levels and melt. The addition of solute effect further limits the number production of ice and causes more precipitation on the ground. Freezing nucleation by bacteria is by far the most efficient nucleation mode. With the same number concentration as dust particles and assuming they all entered cloud water, bacteria can initiate the highest number of ice particles. But the amount of precipitation on the ground is less as compared to the nucleation by mineral dust.

A series of tests on the number concentration effect also suggested that more ice nuclei does not necessarily lead to more precipitation. These preliminary results suggest that in natural clouds the number of ice nuclei may be quite sufficient, and an increase of them either naturally or artificially may cause an “overseeding” to reduce precipitation. In such an “overseeding” regime, solute effect from pollution might enhance precipitation.

A simulation of a lake effect snowstorm around the Great Lakes with a cloud resolving numerical model

Takeshi Maesaka†[1], G. W. Kent Moore[2], Kazuhisa Tsuboki[3]
[1]*National Research Institute for Earth Science and Disaster Prevention, Tsukuba, Japan*
[2]*Department of Physics, University of Toronto, Toronto, Canada*
[3]*Hydrospheric Atmospheric Research Center, Nagoya University, Nagoya, Japan*

1. Introduction

Lake Effect Snowstorm (LES) is well known as a dominant disturbance which brings a heavy snowfall on the leeward of Great Lakes (e.g., Peach and Sykes 1966; Jiusto and Kaplan 1972; Niziol et al 1995). The LES is directly driven by the absolute instability due to cold air outbreaks over the relatively warmer lakes. Therefore LES is usually an aggregate of cellular or roll convections in shallow boundary layer.

The LES has various mesoscale morphologies, like as vortex, shoreline bands, and widespread rolls. Laird et al. (2003a, b) and Laird and Kristovich (2004) examined the factors which affect on the mesoscale morphology, and found that a ratio of wind speed and maximum fetch distance well predicts the morphology. Mann et al. (2002) examined an influence of multiple lake interactions on LES by numerical simulations including/excluding the individual lakes. This study found that the lake distribution affects the location and intensity of LES. Although the LES consists of shallow and small (~1 km) convections, these studies suggested that the Great Lakes scale phenomena (~1000 km) must be also considered to investigate the LES.

The above is way i) small grids width (< 500 m) which can resolve the dynamics of individual convective cells, and ii) a large domain (~1000 km) including whole Great Lakes, are needed to study the LES by using the numerical model. However it has been hard to execute such a heavy simulation because of the shortage of computational resource. In 2002, the Earth Simulator (ES) was developed and started the service by Japan Marine Science and Technology Center (JAMSTEC). The ES is a distributed memory parallel computing system and consists of 640 nodes. Each node has 8 vector processors with shared memory. This new computing system enabled the heavy simulation which resolves the individual convective cells over the Great Lakes.

In this paper, we simulated the LES on 13 January 2003 (Fig. 1) by using a cloud resolving numerical model with the large domain including almost all Great Lakes to examine the predictability of its cloud pattern and quantity of precipitation.

2. LES simulation on 13 January 2003

Figure 1 represents a MODIS true-color satellite image of a LES over the Great Lakes region at 1545 UTC 13 January 2003. The large-scale comma-shaped cloud feature along the southeastern corner of the image is associated with the synoptic-scale cyclone that established the northwesterly flow conducive to the initiation of the LES. At this time, cloud bands occur over and downstream of Lake Superior, Michigan and Huron as well as Georgian Bay. In addition to these bands that are oriented approximately perpendicular to the upwind shore of the lakes, there also exist cloud bands oriented parallel to the upwind shore of western Lake Superior. These bands are associated with gravity waves excited by the flow over topographic feature along this shore (Winstead et al., 2002).

Figure 2 represents the vertically integrated hydrometeor field from the model at 1700 UTC 13 January, the approximate time of the satellite image shown in Fig. 1. The model used in this study is the Cloud Resolving Storm Simulator (CReSS) version 2.1 developed at Nagoya University (Tsuboki and Sakakibara, 2002). This field was calculated by the vertical integration of all 5 hydrometeors contained in the model (cloud water, cloud ice, rain, snow and graupel). This field provides a succinct diagnostic of the characteristics of the clouds in the model. A comparison of Figs. 1 and 2 highlights the fidelity with which the model is able to reproduce the spatial characteristics of the cloud field associated with the LES. In particular, the model is able to simulate the development of the cloud field over and downstream of the Great lakes. For example, the transition from 2D roll to 3D cellular convection, which is often observed to occur in LES, was captured in the model. Distinct band clouds that extend downstream from Lake Huron and Georgian Bay were also simulated successfully. These bands are known as Type I or mid-lake snow bands (Niziol et al., 1995; Laird et al. 2003).

To examine the ability of the model to forecast the precipitation associated with this LES, simulated radar reflectivity fields were calculated from the model hydrometeor fields. Figure 3 shows the comparison of this simulated field with observations at 1309 UTC 13 January 2003 made

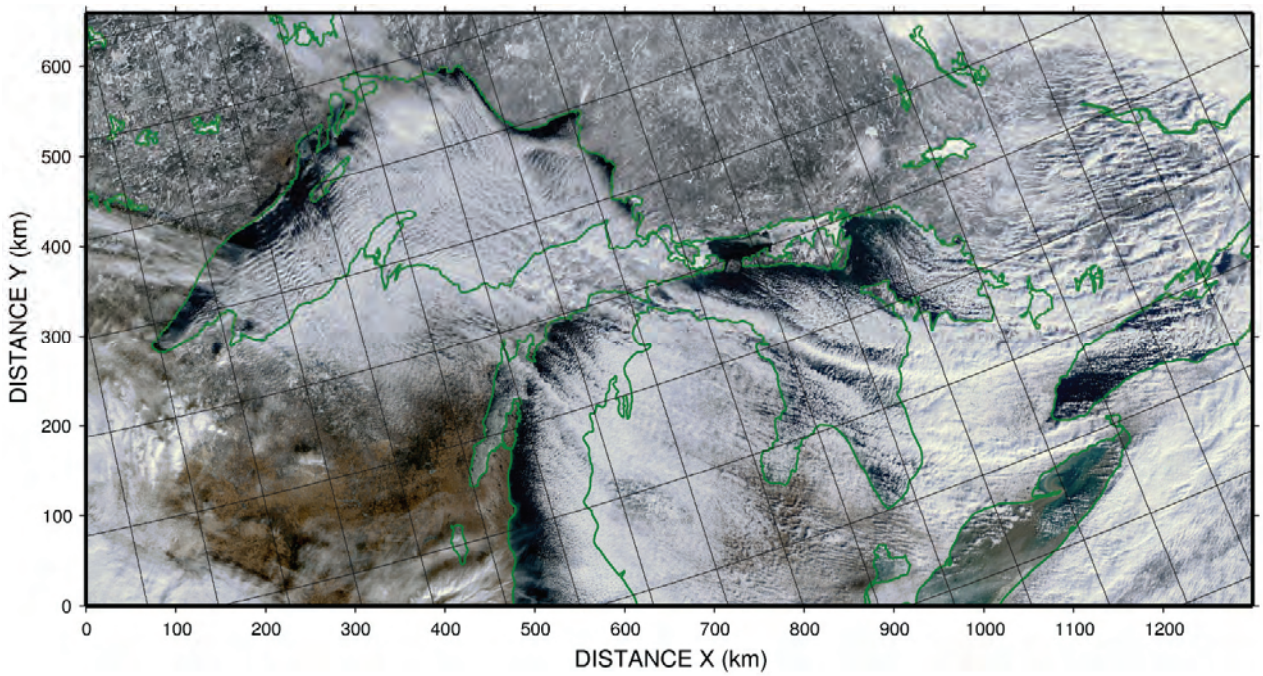

Fig. 1. MODIS true-color satellite image of the Great Lakes region of North America at 1645 UTC 13.

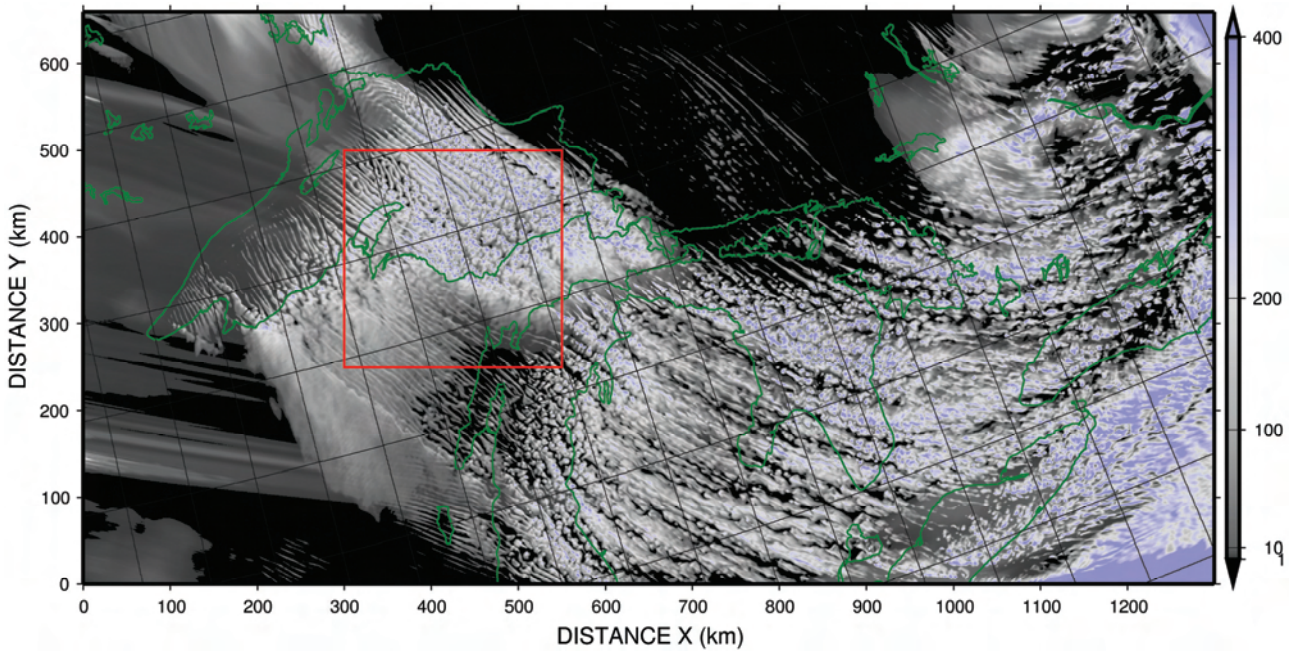

Fig. 2. Vertically integrated hydrometeors (cloud water, cloud ice, rain, snow and graupel) (g m^{-2}) simulated by the numerical model (CReSS). The domain is the same as that shown in Fig. 1. The red rectangle indicates the domain of Fig. 3.

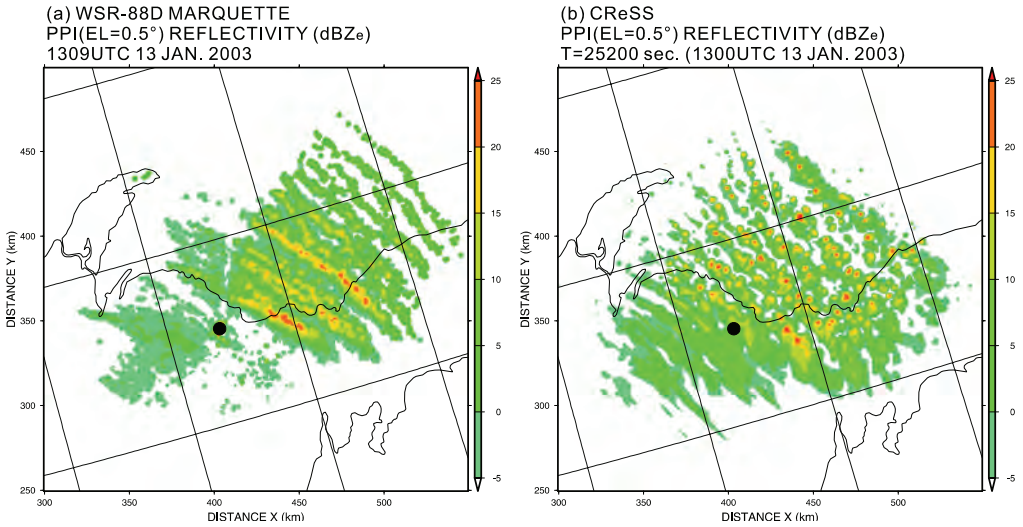

Fig. 3. Radar reflectivity PPI (Plan Position Indicator) image with an elevation of 0.5°. The domain is indicated by the rectangle in Fig. 2. a) Observed by WSR-88D at Marquette, Michigan at 1309 UTC 13 January 2003. b) Simulated by the model at 7 hours after initialization (corresponding to 1300 UTC 13 January 2003).

with the WSR-88D radar at Marquette, Michigan. The maximum observation range of WSR-88D radar is 450 km; however the observation range for the LES are typically only 100-150 km as a result of the shallow nature of clouds and the earth's curvature. As was the case with Figs. 1 and 2, the similarity between the observed and simulated reflectivity fields is striking. In both instances, the bands are aligned with the mean wind, which was from the northwest. Both the observed and simulated reflectivity fields indicate that the bands were well developed over Lake Superior and at this time, tended to become less organized upon landfall. There is also good agreement in the magnitude of the observed and simulated reflectivity. The observed bands tend to narrower and more linear in character as compared to the model bands.

3. Conclusion

In this study, we used a cloud resolving numerical weather model in a large domain to simulate the evolution of a LES that developed over the North American Great Lakes region on January 13th, 2003. The simulation succeeded to reproduce the important natures of LES, such as the transition from 2D roll to 3D cellular convections and the mid-lake snow band. The simulated snowfall intensity in the model coincided with that of radar observation. The results of this study suggest that it is possible to such models to produce realistic simulations of mesoscale weather systems such as LES that develop as the result of the interaction of synoptic-scale and cloud-scale circulations in the presence of varying surface conditions.

References

Jiusto, J. E., and M. L. Kaplan. 1971: Snowfall from lake-effect storm. Mon. Wea. Rev., 100, 62-66.

Laird, N. F., D. A. R. Kristovich and J. E. Walsh, 2003a: Idealized model simulations examining the mesoscale structure of winter lake-effect circulations. Mon. Wea. Rev., 131, 206-221.

Laird, N. F., J. E. Walsh and D. A. R. Kristovich, 2003b: Model simulations examining the relationship of lake-effect morphology to lake shape, wind direction, and wind speed. Mon. Wea. Rev., 131, 2102-2111.

Laird, N. F. and D. A. R. Kristovich, 2004: Comparison of observations with idealized model results for a method to resolve winter lake-effect mesoscale morphology. Mon. Wea. Rev., 132, 1093-1103.

Mann, G. E., R. B. Wagenmaker and P. J. Sousounis, 2002: The infuluence of maultiple lake interaction upon lake-effect storms. Mon. Wea. Rev., 130, 1510-1530.

Niziol, T. A., W. R. Snyder and J. S. Waldstreicher, 1995: Winter weather forecasting throughout the Eastern United Status. Part IV: Lake effect snow. Wea. Forecasting, 10, 61-77.

Peach, Jr., R. L. and R. B. Sykes, Jr., 1966: Mesoscale study of a lake effect snow storm. Mon. Wea. Rev., 94, 495-507.

Tsuboki, K and A. Sakakibara, 2002: Large-scale parallel computing of Cloud Resolving Storm Simulator. High Performance Computing, Springer, H. P. Zima et al. Eds, 243-259.

Winstead, N. S., T. D. Shikora, D. R. Thompson and P. D. Mourad, 2002: Direct influence of gravity waves on surface-layer stress during a cold air outbreak, as shown by synthetic aperture radar. Mon. Wea. Rev., 130, 2764-2776.

Verification of solid precipitation using radar simulator for JMA nonhydrostatic model

Yasutaka Ikuta
Numerical Prediction Division, Japan Meteorological Agency,
1-3-4, Otemachi, Chiyoda-ku, Tokyo 100-8122, Japan

We are developing a volume verification method of three-dimensional distribution of liquid or solid water particles for the operational non-hydrostatic meso-scale model (MSM) at the Japan Meteorological Agency (JMA). The volume verification helps us understand the forecast characteristic of hydrometeors. It also contributes to providing information for an airplane safety operation and disaster prevention through the improvement in the representation of hydrometeors distribution.

The volume verification method makes use of a radar simulator. This radar simulator provides an equivalent reflectivity factor Z_e, Doppler velocity V_r and beam-path position. The Z_e was computed from the size-distribution of precipitation particles on beam-path through the geometry of the pointing angle of the virtual antenna in the MSM forecast. The V_r was calculated from the air motion and the mass-weighted terminal velocity of precipitation on that beam-path. The beam-path was calculated from a refractive index of reproduced atmosphere and the curvature of the earth. The estimates of position by simulated beam-path provide the plan position indicator (PPI) for each elevation from the MSM forecast. The PPI make it possible to compare the forecast with the radar observation, because the observed beam-path has uncertainty of three-dimensional position. The precipitation particles on beam-path were three types of precipitating hydrometeors which is rainwater, snow and graupel. Those size-distributions were diagnosed by the one-moment scheme of bulk microphysics parameterization, similar to the scheme of the MSM.

In order to compare these simulated elements, we have applied a Fractions Skill Score (FSS) approach (Roberts and Lean, 2008) to the volume verification. The FSS is one of the several fuzzy verification methods of relaxing requirement of perfect time-space matching. These methods are more appropriate to estimate displacement error than traditional verification approaches.

A case study on 7 February 2008 was made using the radar simulator for the demonstration of volume verification. Figure 1 shows a comparison between the simulated Z_e and the observation, and the value of its FSS. For absolute threshold 20 dBZ FSS had been under the target skill, because the frequency bias is large. In contrast, for 99th percentile threshold (localized reflectivity) FSS became larger than the target skill in the large spatial scale. The forecast of such score can be regarded as a useful forecast, if the displacement error comparable to the spatial scale has been permitted. As a result of study, it turned out that the MSM forecasts weak reflectivity widely in a snowfall region. However, this wide spread representation of weak reflectivity was improved by inclusion of a prognostic equation for number concentration of snow particles into the two-moment experimentally. Additionally, it was indispensable to consider the displacement error in verification of the high reflectivity.

We conclude that it is expected that volume verification using the radar simulator and FSS approach will enable quantitative comparison of three-dimensional precipitation particle distribution.

References

Roberts, N.M. and H.W. Lean, 2008: Scale-selective verification of rainfall accumulations from high- resolution forecasts of convective events. *Mon. Wea. Rev.*, **136**, 78-97.

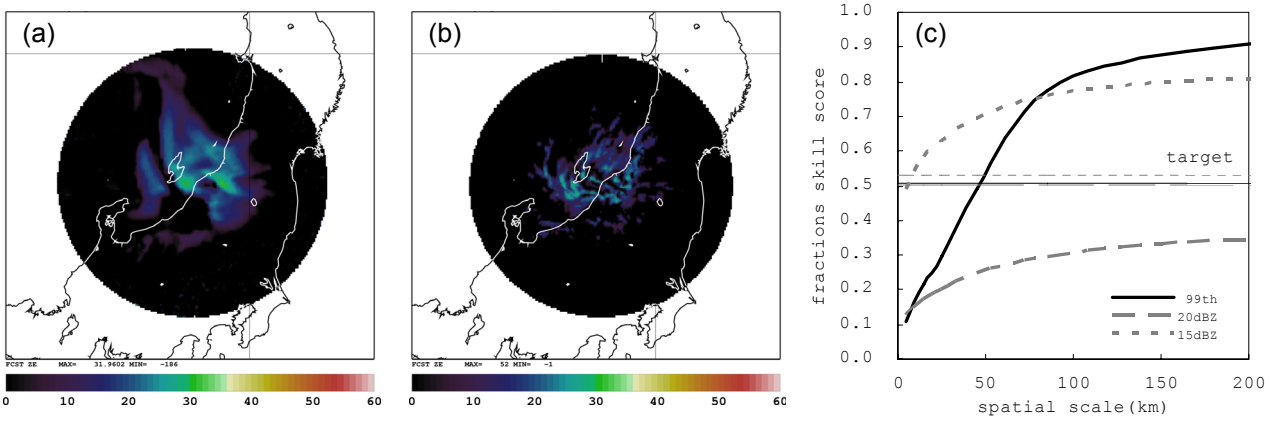

Fig. 1. Equivalent Reflectivity factor (dBZ) of the 0.0° elevation for (a) the radar simulator and (b) the observation at 0600 UTC 7 February 2008. The center of the map shown is the Niigata radar operating by JMA, and (c) FSS is computed from comparison between (a) and (b).

Characteristics of cloud microphysics in the JMA nonhydrostatic model on solid precipitation forecast

Masashi Ujiie
Numerical Prediction Division, Japan Meteorological Agency
1-3-4 Otemachi Chiyoda-ku Tokyo 100-8122, Japan

1 Introduction

The Japan Meteorological Agency(JMA) has been operating a nonhydrostatic meso scale model (MSM) with the horizontal grid spacing of 5km. The main purpose of the operation is to provide information contributing to preventing natural disasters such as heavy rain and snow.

The JMA is also developing a model with the finer horizontal grid spacing of 2km to contribute to the aviation forecast and more detailed information for disaster prevention. We call the model LFM (Local Forecast Model). As a part of the development, the Numerical Prediction Division of the JMA has operated the LFM experimentally since July 2007. The computational domain of the experiment covers with $300 \times 300\text{km}^2$ area (red solid square in Figure 1). It includes a plain facing the Pacific Ocean where heavy snow events rarely occur. Through the experimental operation, we have found that the LFM is superior to the MSM in prediction of heavy rain. We are planning to extend the computational domain for next experiment. The Sea of Japan side of the Japan Islands, where heavy snowfall events often occur, is going to be included in the domain. Snowfall events will be important forecast objectives. We should understand characteristics of the LFM on solid precipitation through some case studies.

Purposes of this presentation are to investigate (i)how the LFM can represent snow cloud and fall compared to observation and the MSM, (ii)what differences of characteristics of water content between the LFM and the MSM are.

2 Forecast models

Both forecast models of the LFM and the MSM are based on JMA-NHM(Saito et al. 2006). The differences between the two models are their resolution and moist processes. The MSM uses cloud microphysics (Lin et al. 1983; Murakami 1990) together with Kain-Fritsch (KF) type cumulus convective parameterization because the horizontal grid spacing of 5km is too coarse to represent cumulus convection explicitly. On the other hand, the LFM with higher horizontal grid spacing of 2km uses only the cloud microphysics to represent convection explicitly.

3 Case study

A snowfall event occurred around the Sea of Japan side of Japan Islands on 9 January 2009. The daily amount of snowfall on 10 (15UTC 9 to 15UTC 10) January 2009 was recorded 67cm at Daisen(located at the altitude of 875m), and 32cm at Tottori (located at the altitude of 7.1m) observatory stations (Figure 1). The synoptic situation showed an upper trough and cold air were located over western side of the Japan Islands. The lower atmosphre was warm and moist. Thus, the atmosphere was potentially unstable over the region (Figure 2).

Figure 3 show accumulated precipitation of observation, the MSM and the LFM from 18-21UTC 9 January 2009. Both of the models can represent precipitation around the northeastern side of the surface convergence line, and a snowfall along the Chugoku Mountains well. But the models tend to precipitate snow more than observation on the Chugoku Mountains. Though precipitation represented by the two models is similar to the observation, the water content in the atmosphere differs between the two. Figure 4 shows forecasted vertically integrated snow at 21UTC 9 January 2009. The MSM forecasts the snow broadly. The distribution of the snow cloud is corresponding to the region where the level of neutral buoyancy is high. When cloud ice generated by the KF scheme is removed as a sensitive study, the amount of the snow cloud was reduced (not shown). This result suggests that the broad snow cloud was converted from cloud ice with the help of the KF scheme and the KF scheme is sensitive to the static stability of the mosit atmosphere. On the other hand, the LFM concentrates the snow cloud and cloud water around the northeastern side of the surface convergence line. The alignment of cloud clines and positive vertical velocity are perpendicular to the surface convergence line and parallel to the vertical wind shear vector (Figure 5). The convective patterns are qualitatively similar to eigen modes derived from linear theories (Asai 1970; Asai 1972). That suggests the LFM represents the snow cloud and the convection explicitly.

4 Summary and future plans

In the case study, both the MSM and the LFM can represent total precipitation well comparing with the observation. However, both of the models tend to be sensitive to the orography and to concentrate much snowfall on the mountain. The structure of the cloud differs between the two models. The main causes of the difference seem to the sensitivity of the KF scheme to the static stability of the moist atmosphere, and explicit/implicit expression of the convection. The convective pattern forecasted by the LFM is qualitatively consistent with eigen modes derived from the linear theories. In the future, we have to investigate more cases and verify statistically through the next experimental operation to identify whether these characteristics are general or not.

References

Asai, T., 1972: *J. Meteor. Soc. Japan.*, **50**, 525-532

Lin, Y.-L. et al., 1983: *J. Climate. Appl. Meteor.*, **22**, 1065-1092

Murakami, M., 1990: *J. Meteor. Soc. Japan.*, **68**, 107-128

Saito, K. et al., 2006: *Mon. Wea. Rev.*, **134**, 1266-1298

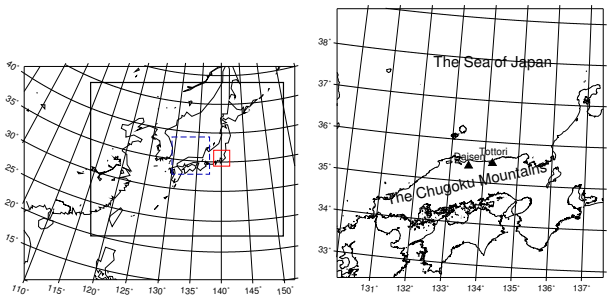

Figure 1: Left:computational domains of the MSM(thick solid square colored by black), the LFM for the experimental operation(thin solid square colored by red), and the LFM for this presentation(thin dashed line colored by blue). Right: detailed map of the computational domain for the LFM.

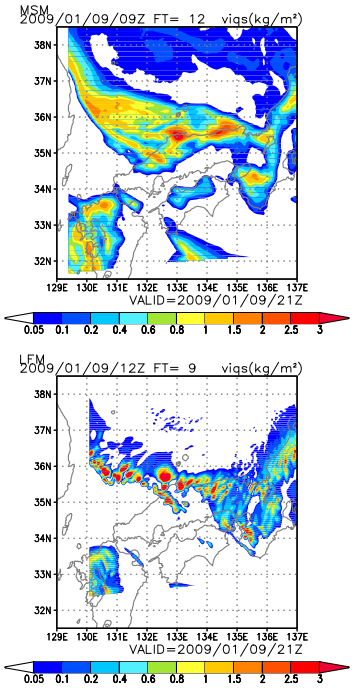

Figure 4: Vertically intergrated snow in the atmosphere at 21 UTC 9 January 2009. Top: the MSM. Bottom: the LFM

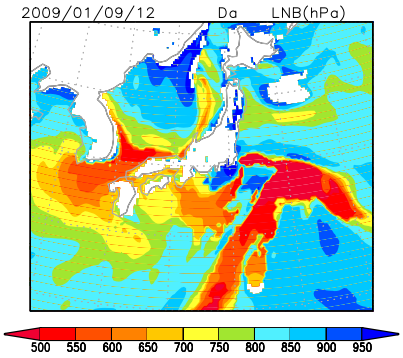

Figure 2: Level of neutral buoyancy (hPa, approximating potential level of cloud top) at 12UTC 9 January 2009

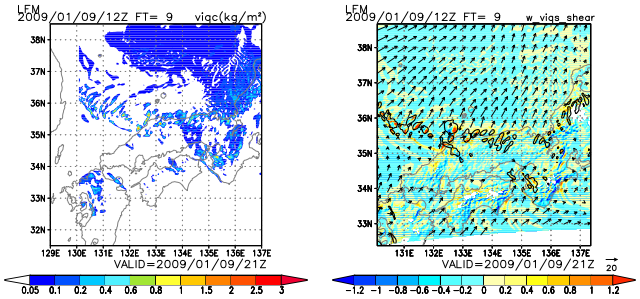

Figure 5: Left: Vertical integrated cloud water in the atmosphere, Right:Vertical velocity at the height of 1000m (m/s, shade) and difference of wind vector between the height of 3000m and 100m (m/s, vector) at 21UTC 9 January 2009.

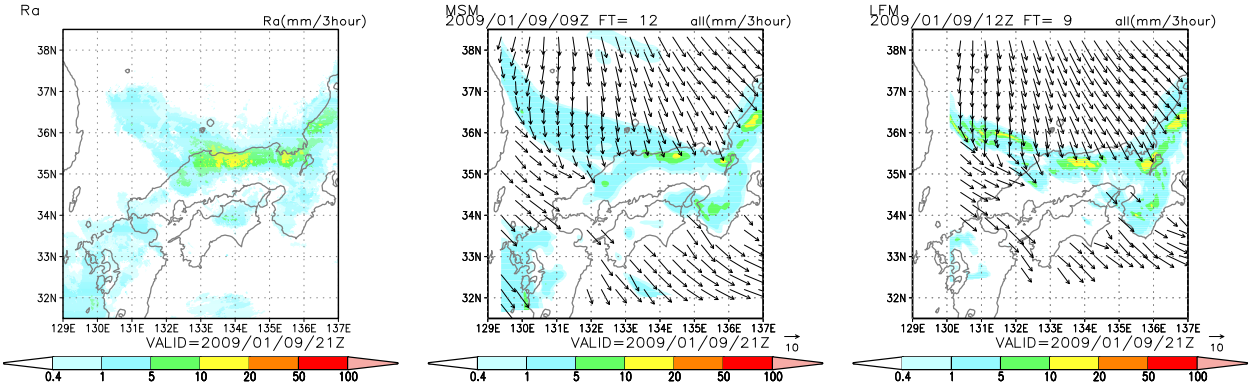

Figure 3: Accumulated precipitation from 18-21UTC on 09 March 2009. Left: Observation(derived from radar data corrected by rain gauge data). Center:the MSM. Right: the LFM

Comparison of CRM and surface/radar observations

Sento Nakai[1]
[1]*Snow and Ice Research Center, NIED, Nagaoka, Japan*

1. Introduction

Quantitative evaluation is necessary on the prediction of winter meteorological conditions especially when snowfall happens for disasters related to avalanche and blizzard depend on the small-scale meteorological conditions. The snowfall is also important as water resources in the warm season.

The author and co-workers have compared winter precipitation distributions between radar observations and simulations using a cloud-resolving model (CRM). The simulation successfully reproduced the difference among the features of various winter precipitating cloud systems during the heavy snowfall in December 2005. Although the simulated precipitation variation in a coastline- perpendicular direction seemed quantitatively well reproduced in a level of 1500 m, a large discrepancy was found in the vertical profile of precipitation in levels below 1500 m. While radar-based snow water equivalent (SWE) increased with decreasing height, simulated SWE decreased with decreasing height below 1500 m. The excessive evaporation was suggested in the simulated atmosphere for the comparison with surface observation indicated the underestimation of precipitation and relative humidity. However, they used a fixed relation between precipitation intensity (R) , terminal fall velocity of snow particles (Vt), and equivalent radar reflectivity factor (Ze). The downward increase of Ze may be affected by the change of these relations in the real precipitation.

In this study, the author describes the results of a comparison of simulation data using a CRM and radar/surface observation data. A period during 12 to 18 February 2008 was selected as an analysis period. A continuous snowfall was observed associated with a developing low pressure system and the succeeding outbreak of a winter monsoon in the analysis period.

2. CRM simulations

Numerical simulation of snowfall for the analysis period was carried out at the Snow and Ice Research Center (SIRC), National Research Institute for Earth Science and Disaster Prevention (NIED) through the double nesting of JMANHM. The JMANHM is a non- hydrostatic mesoscale model for research and operational use developed at the Numerical Prediction Division (NPD) of the Japan Meteorological Agency (JMA) and the Meteorological Research Institute (MRI). Details of the JMANHM are described in Saito et al. (2006).

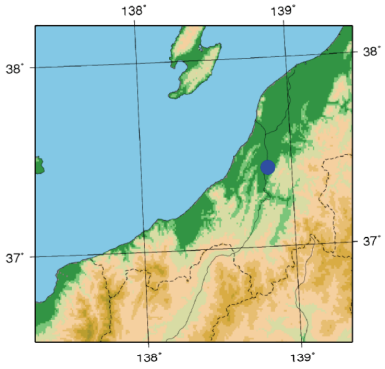

Fig. 1 Domain of the inner model. A solid blue dot indicates the place of this workshop.

Lambert Conformal projection and the terrain-following vertical coordinate system were used for both inner and outer models. The horizontal resolution of outer (inner) model was 10 km (1.2 km). The area of the inner model is shown in Fig. 1. An explicit 2-moment 3-ice bulk cloud microphysics scheme was used in both models. A convective parameterization scheme was not used in both models. The simulation was executed using operational Meso-Scale Model (MSM) forecast as initial and boundary conditions of the outer model. The 3-hour forecast and the succeeding forecast data of the outer model were used as the initial and boundary conditions of the inner model. Data of the inner model of 9 to 20 hour from the initial time of the MSM in 1-hour intervals were used for the analysis.

3. Observation data

The CRM simulation was compared with surface station data and radar observations. The data of SIRC observation field and 18 JMA stations (the Automated Meteorological Data Acquisition System: AMeDAS) were used as the surface station data. The lack of data was treated basically in accordance with the JMA guideline and was taken into consideration in the comparison with the simulation.

The simulated mixing ratio of snow (graupel) particles Qs (Qg) (g kg^{-1}) was compared with Ze (dBZ) observed by the XPOL radar (Iwanami et al., 1996) located at SIRC. The Qp was the sum of the mixing ratios of rain, snow and graupel. The Ze was on a Cartesian coordinate system in a horizontal (vertical) resolution of 1 km (500 m) converted from 12-elevation volume scan data in 10-minute intervals.

4. Comparison results

4.1 surface meteorological elements

A comparison of the simulation and surface observation of 19 stations (18 JMA stations and

SIRC) was made. Mean error (ME) and root mean square error (RMSE) of surface meteorological elements were calculated. The ME of temperature was between 0.5 K and 1K at many points except three coastal stations (ME ~ 0 K) and two inland stations (ME <0K). Many of the stations showed negative bias in simulated daily precipitation between -5 mm and 0 mm, except four stations located near or between mountains. No station showed ME of more than 1 mm in daily precipitation. The average values of 19 stations were:

	ME	RMSE
Temperature	0.43	1.41
Daily precipitation	-4.78	10.01

4.2 precipitation

The precipitation during the analysis period was manually divided into 14 cases using the Ze distributions in a level of 1500 m. Each case was classified to a specific type of mesoscale precipitating cloud system (Nakai et al. 2005).

Case 11 was a period of meso-beta scale vortices moving in west-east direction and accompanied by a significant change of wind direction in the Doppler velocity field after the passage (Fig. 2a). The prevailing snow particle type was rimed snowflakes and aggregates according to the observation at SIRC. Similar snowbands in the same west-east running direction were reproduced in the simulation although the time evolution of the cloud features was several hours earlier than observation. Figure 3a is a west-east vertical section of Qs and Qg averaged in the north-south direction over a box surrounding the snowband. The Qs was larger than Qg by one order of magnitude. It seems that the composition of the precipitation particles was well simulated.

Case 5 was a period of longitudinal snowband moving in a direction of west-northwest to east-southeast (Fig. 2b). Graupels dominated the precipitation particles according to the observation at SIRC. Longitudinal snowbands were reproduced although the running direction was slightly different. Figure 3b is a west-east vertical section of Qs and Qg averaged in the north-south direction over a box surrounding the snowband. The Qs was much larger than Qg. It is obviously different from observed characteristics of precipitation particles.

5. Summary

The results of numerical simulations were compared with surface station data and radar observations for the period of one week in the middle of February 2008. The simulation result is applicable to the point-to-point comparison although there are problems to be solved for the quantitative reproduction of meteorological variables. Heat, moisture and momentum transport in the surface boundary layer should be re-examined for the simulation of the station data. The quantitative validation on microphysical characteristics of each type of precipitating cloud systems is essential to the improved prediction and radar estimation of solid precipitation.

Acknowledgments: This work is supported by a project of the National Research Institute for Earth Science and Disaster Prevention titled "Research project for developing a snow disaster forecasting system and snow hazard maps." GrADS (Grid Analysis and Display System) was used to draw some of the figures.

References

Iwanami, K., M. Maki, T. Sato and M. Higashiura, 1996: Distribution of precipitation parameters estimated from observations with a Doppler radar and a polarimetric radar: Part 2, Results from polarimetric radar observation. Proceedings, 12th International Conference on Clouds and Precipitation, 190-192.

Nakai, S., K. Iwanami, R. Misumi, S.-G. Park and T. Kobayashi, 2005: A classification of snow clouds by Doppler radar observations at Nagaoka, Japan. SOLA, 1, 161-164.

Saito, K., T. Fujita, Y. Yamada, J. Ishida, Y. Kumagai, K. Aranami, S. Ohmori, R. Nagasawa, S. Kumagai, C. Muroi, T. Kato, H. Eito and Y. Yamazaki, 2006: The operational JMA nonhydrostatic mesoscale model. Mon. Wea. Rev., 134, 1266-1298.

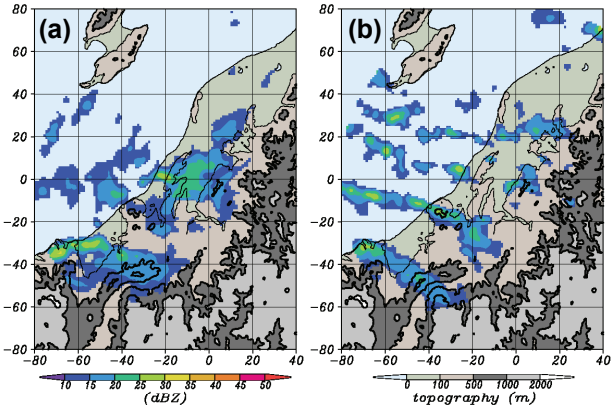

Fig. 2. Ze distribution in a level of 1500 m. Absscissa and ordinate are the distance from radar located at SIRC. (a) 1723 JST February 16, 2008, and (b) 0003 JST February 14, 2008.

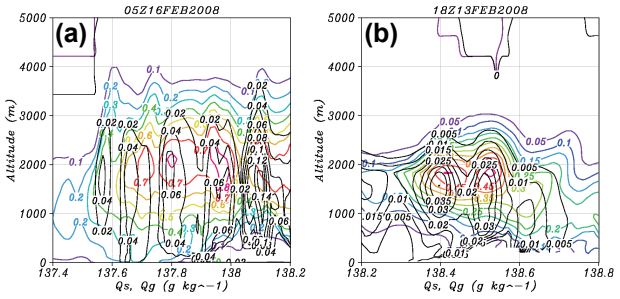

Fig. 3. West-east vertical sections of Qs and Qg averaged in the north-south direction over a box surrounding snowbands. (a) 05 JST February 16, 2008, and (b) 18 JST February 13, 2008.

Hydrometeor type classification in winter clouds using X-band polarimetric radar measurements

Koyuru Iwanami *[1], Kenichi Kusunoki [2], Narihiro Orikasa [2],
Masayuki Maki [1], Ryohei Misumi [1], and Masataka Murakami [2]
[1] *National Research Institute for Earth Science and Disaster Prevention (NIED), Tsukuba, Japan*
[2] *Meteorological Research Institute, Tsukuba, Japan*

1. Introduction

Hydrometeor type classification in precipitation clouds is useful for not only study of precipitation mechanisms but also disaster prevention by monitoring and/or forecast of hail and lightning, discrimination between rain and snow, and improvement of weather forecast through data assimilation. Polarimetric radar measurements of precipitation can be used effectively to classify hydrometeor types in precipitation because they are sensitive to the hydrometeor properties. Hydrometeor type classification using the fuzzy logic techniques has been proposed and there are two models of the product method (Liu and Chandrasekar 2000) and the additive method (Zrnić et al. 2001) in the interference stage of fuzzy logic classification system. Recently Lim et al. (2005) proposed a hybrid model that combined the additive method and the product method.

In order to develop hydrometeor classification method using X-band polarimetric radar measurements, simultaneous observations were carried out by the NIED X-band polarimetric radar (MP-X; Iwanami et al. 2001) and the hydrometeor videosondes (HYVIS; Murakami and Matsuo, 1990) in Niigata prefecture, Japan in December 2001. Characteristics of polarimetric measurements and temperature for five hydrometeor types were derived from comparisons of the MP-X and the HYVIS data. The beta membership functions in the fuzzification process of the fuzzy logic classification were specified based on the derived characteristics of polarimetric measurements for each hydrometeor type. Results of hydrometeor classification using fuzzy logic technique including a hybrid rule strength (Lim et al. 2005) and its verification are presented.

2. Observation and data

Simultaneous observation was carried out by the NIED X-band polarimetric radar (MP-X; Iwanami et al. 2001) and the hydrometeor videosondes (HYVIS; Murakami and Matsuo, 1990) in Niigata prefecture, Japan for three weeks in December, 2001 by the National Research Institute for Earth Science and Disaster Prevention (NIED) and the Meteorological Research Institute (MRI). MP-X radar site located on the southeastern slope of the Uonuma hills. Radar data were collected in the southeastern area of the site within 30 km range.

The balloons equipped with the hydrometeor videosonde (HYVIS) and a rawinsonde were launched at the surface meteorological observation site located 2.2 km southeast from the radar site.

Main specifications of the NIED X-band polarimetric radar, MP-X (Iwanami et al. 2001), mounted on a 4-ton truck are listed in Table 1. Radar data were collected by RHI scans during HYVIS observations considering their tracks. The range and angle resolutions and number of pulse integration was 100 m, 0.5 degree and 256, respectively. The dwell time for one RHI scan was about 38 sec. The polar coordinate data by RHI scans were transformed to the Cartesian coordinate data with 500 m horizontal and 250 m vertical resolutions. Polarimetric measurements of reflectivity at horizontal polarization (Z_H), differential reflectivity (Z_{DR}) and correlation coefficient (ρ_{HV}) were mainly analyzed.

Table 1. Specifications of the NIED MP-X radar.

Frequency	9.375 GHz
Beam Width	1.3 degree
Peak Power	50 kW
Pulse Width	0.5 μs
PRF	≤ 1,800 Hz
Polarization	SHV
Observation Range	≤ 80 km
Outputs	Z_H, V, W, Z_{DR}, ρ_{HV}, Φ_{DP}, K_{DP}

The hydrometeor videosonde (HYVIS) has been developed to measure the vertical distribution of hydrometeors in clouds by Murakami and Matsuo (1990). Two small TV cameras in the HYVIS take pictures of hydrometeors. The HYVIS and a rawinsonde are attached to the same balloon and launched into clouds, so that both particle images and meteorological data are collected simultaneously.

Fifteen balloons equipped with the HYVIS systems were launched during the field experiment and the data of nine HYVIS launches could be analyzed together with radar data. One-hour precipitation amounts and air temperature on the surface around their launch times were from 0 to 1.0 mm and from 0.1 to 6.9 °C, respectively.

The HYVIS data of the position, air temperature, and hydrometeor type were utilized in this analysis. Although hydrometeor types were at first classified into eight categories of water drop (R), sleet (S), graupel (G), aggregate (A), dendrite (D), column (C), plate (P), and needle (N) from the particle images, D, C, P, and N were classified into one category of single ice crystal (X) in the following analysis.

3. Characteristics of polarimetric measurements for hydrometeor types

Characteristics of polarimetric measurements of reflectivity at horizontal polarization (Z_H), differential reflectivity (Z_{DR}) and correlation coefficient (ρ_{HV}) and temperature (T) for five hydrometeor types, that is, water drop (R), sleet (S), graupel (G), aggregate (A) and ice crystal (X), were derived from comparisons of MP-X and HYVIS data.

The position of HYVIS was compared with the plane of RHI scan, then the sets of radar and HYVIS data were picked up on conditions that the time difference was less than 3 minutes and the horizontal distance between the position of the HYVIS and the plane of RHI scan was less than 1.5 km.

Table 2 shows the number of HYVIS image data for each hydrometeor type picked up for comparisons between polarimetric measurements and hydrometeor types on the conditions described above. There were a few hydrometeor types in one HYVIS image in many cases. In such cases, those different hydrometeor types were compared with the same polarimetric parameters in one mesh on RHI data, that is, the numbers in the column 'Multi' in Table 2 include overlap. If another condition that there was only one type of hydrometeor in one HYVIS image was added, the numbers of HYVIS image data decreased by 4 (A) to 54 % (R) shown in the column 'Single' in Table 2.

Table 2. The number of HYVIS image data for each hydrometeor type. See text.

Hydrometeor Type	Number of HYVIS Image Data	
	Multi	Single
: Water Drop	485	262
S: Sleet	188	67
G: Graupel	973	198
A: Aggregate	326	12
X: Ice Crystal	2179	589
Total	4151	1128

Frequency that each polarimetric parameter and air temperature has some value was derived from comparing picked-up radar and HYVIS data for each hydrometeor type.

4. Hydrometeor type classification

For hydrometeor type classification, fuzzy logic technique including a hybrid model proposed by Lim et al. (2005), which combined the additive method and the product method in the interference stage, was used. The beta membership functions, that are important for classification performance, were specified based on the derived characteristics of polarimetric measurements for each hydrometeor type described in section 3.

Figure 1 shows an example of the results of the hydrometeor type classification with the RHI images of polarimetric measurements of Z_H, Z_{DR}, and ρ_{HV} at 07:35:46 LST December 16, 2001. Each width of the beta membership function was set to the range of 70 % of accumulated frequency of polarimetric measurements and temperature from the maximum(s) to both sides.

The hydrometeor types detected by HYVIS and classified by the method were compared for validation. The rates of 'hits' to 'false alarm' for type R, S, G, A, and X were 70, 39, 58, 0, and 69 %, respectively. The reasons why it was more difficult to identify correctly aggregate (A) were considered that aggregate (A) was detected

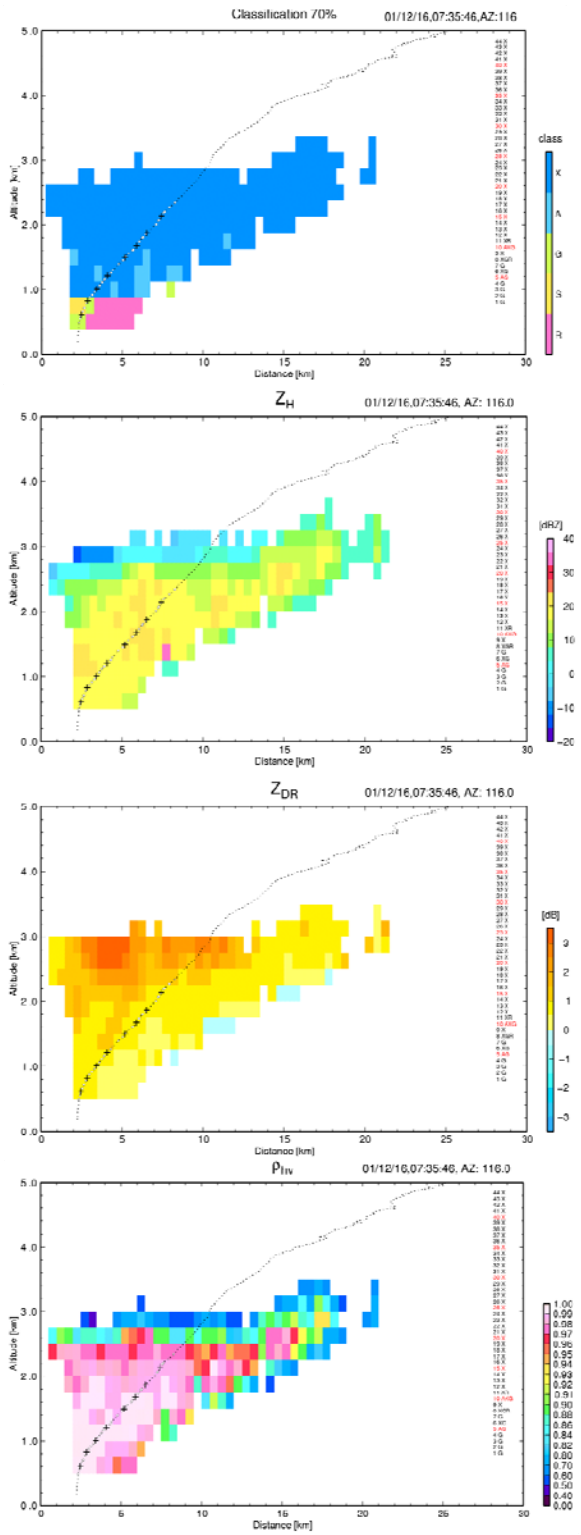

Fig. 1. Hydrometeor classification result and RHI images of Z_H, Z_{DR}, and ρ_{HV} at 07:35:46 JST on Dec. 16, 2001. Dotted line, marks of open circle and cross show the HYVIS track and the positions of HYVIS image data, respectively.

together with the other types of hydrometeor in almost all HYVIS images, and ice crystal (X) include originally four kinds of hydrometeors with different characteristics of particles then with wide range of polarimetric measurements in snow clouds. The aggregate (A) and ice crystal (X) should be included in one category of dry snow at present.

5. Summary and issues

X-band polarimetric radar data were collected simultaneously as *in-situ* measurements with hydrometeor videosonde (HYVIS) in winter clouds. Both data were compared and frequency polygons of polarimetric measurements and temperature for hydrometeor types were derived. Results of hydrometeor classification using fuzzy logic technique including a hybrid rule strength (Lim et al. 2005) and its verification were also reported. The beta membership functions were specified based on the derived characteristics of polarimetric measurements and temperature for each hydrometeor type.

In-situ observation data by the Instrumented aircraft can be utilized for validation of the classification method.

Acknowledgements. The authors would like to acknowledge Dr. S.-G. Park for supporting radar observation.

References

Iwanami, K., R. Misumi, M. Maki, T. Wakayama, K. Hata, and S. Watanabe, 2001: Development of a multiparameter radar system on mobile platform. *Proc. 30th Intern'l Conf. Radar Meteor.,* 104-106.

Lim, S., V. Chandrasekar, and V. N. Bringi, 2005: Hydrometeor classification system using dual-polarization radar measurements: Model improvements and in situ verification. *IEEE Trans. Geosci. Remote Sensing*, **43**, 792-801.

Liu, H., and V. Chandrasekar, 2000: Classification of hydrometeors based on polarimetric radar measurements: Development of fuzzy logic and neuron-fuzzy systems, and in situ verification. *J. Atmos. Oceanic Technol.*, **17**, 140-164.

Murakami, M., and T. Matsuo, 1990: Development of hydrometeor videosonde. *J. Atmos. Oceanic Technol.*, **7**, 613-620.

Zrnić, D. S., A. Ryzhkov, J. Straka, Y. Liu, and J. Vivekanandan, 2001: Testing a procedure for automatic classification of hydrometeor types. *J. Atmos. Oceanic Technol.*, **18**, 892-913.

Observation and simulation on hydrometeor properties of snow clouds

Tadayasu Ohigashi, Kazuhisa Tsuboki, Yukari Shusse, Masaya Kato,
Taro Shinoda, and Hiroshi Uyeda
Hydrospheric Atmospheric Research Center, Nagoya University, Nagoya, Japan

1. Introduction

Structure and evolution of hydrometeor properties as well as those of dynamics are important to understand precipitation systems. Cloud resolving models, which represent complicated microphysical processes, are a powerful tool to examine microphysical properties. On the other hand, polarimetric radar can obtain 3-dimensional information of microphysical properties such as shape, phase, and attitude of particles, and is a useful instrument to observe hydrometeor properties. Some hydrometeor classification methods have been recently developed using polarimetric parameters.

A polarimetric radar of Nagoya University was installed from December 2008 to March 2009 in Hokuriku, which is located in the coastal region of central Japan, to observe snow clouds over the Sea of Japan during cold air outbreak. Daily numerical simulation is also performed during the observation period. In this study, a case study is shown to compare hydrometeor properties in observation with numerical simulation result.

2. Observation and daily numerical simulation

New X-band polarimetric radars were introduced in November 2007 to Nagoya University. In the winter from December 2008 to March 2009, a polarimetric radar with a frequency of 9375 MHz (X-band) is installed at Oshimizu, Ishikawa of Hokuriku. The radar is referred to as "Oshimizu radar." The specifications of Oshimizu radar is shown in Table 1. Oshimizu radar was operated with 12 Plan Position Indicator (PPI) scans in 5 minutes, and Range Height Indicator (RHI) scans were occasionally performed by manual operation.

During the observation period, numerical simulation was daily performed using Cloud Resolving Storm Simulator (CReSS) developed by Nagoya University (e.g., Tsuboki and Sakakibara 2002). The domain has $260 \times 240 \times 26$. A horizontal resolution is 5 km. Variable vertical grid intervals with 150 m at the bottom are used and its average interval is 500 m. A microphysical process is formulated by a bulk method of cold rain parameterization. Hydrometeor types included in the model is cloud, rain, ice, snow, and graupel. These mixing ratios and solid hydrometeors' number densities are predicted.

Table 1 Specifications of the Nagoya University polarimetric radar installed at Oshimizu.

Frequency	9375 MHz
Peak power	200 W
Pulse length	32 μs
Pulse compression	chirp(FM)
PRF	500 to 2000 Hz
Antenna diameter	2.0 m
Beam width	1.2°
Polarimetric wave	45°
Parameters	Z_{hh}, Z_{vv}, V, W, ϕ_{DP}, $\rho_{hv}(0)$, Z_{DR}, K_{DP}

3. Case study of a broad cloud band

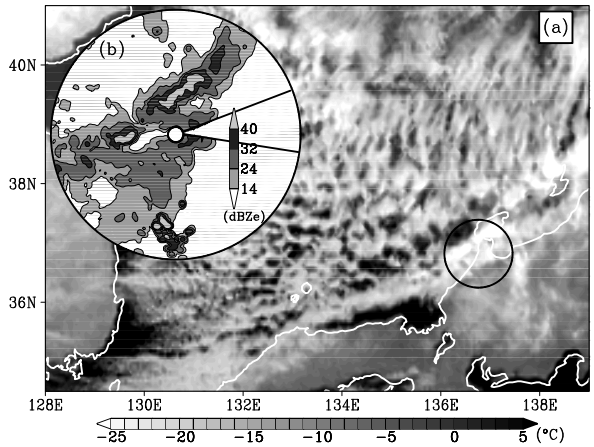

Fig. 1 (a) MTSAT infrared-1 image at 06 JST, 25 January 2009. The circle shows observation range of Oshimizu radar. (b) Radar reflectivity (dBZe) at a height of 1 km at 0530 JST, 25 January 2009.

During cold air outbreaks from 24 to 27 January 2009, the westerly to west-southwesterly wind was maintained in the western Sea of Japan. Figure 1a shows a satellite image at 06 JST (Japan Standard Time), 25 January 2009. A cloud band formed near the coast along the westerly to west-southwesterly wind in the western Honshu Island. The width of the cloud band was wider than the other cloud bands. At the landing part of the broad cloud band, brightness temperature is much low. This indicates localized development of the cloud band at the landing part. This development occurred within the

observation range of Oshimizu radar. Figure 1b shows radar reflectivity at a height of 1 km. The reflectivity more than 40 dBZe is seen, which corresponds to low brightness temperature region shown in Fig. 1a. This reflectivity value is strong for clouds during cold outbreaks.

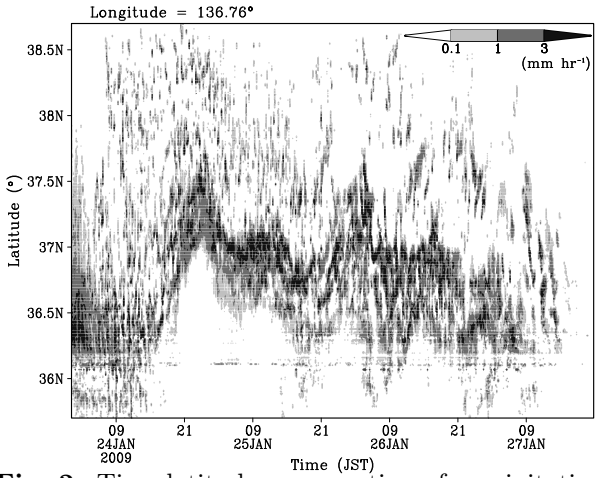

Fig. 2 Time-latitude cross section of precipitation intensity (mm hr^{-1}) of JMA radar along a longitude of 136.76°E. This longitude corresponds to the landing part of the broad cloud band.

Figure 2 is time-latitude cross section of precipitation intensity (mm hr^{-1}) of JMA radar along the landing part of the broad cloud band. Although the cloud band slightly moves to the south, the broad cloud band was located between 36.5°N and 37°N from 00 JST, 25 to 09 JST, 27 January 2009.

The daily simulation results successfully reproduced the cloud band, although the cloud band in the simulation was not stagnant for a long time. The banded updraft extends toward Hokuriku (Fig. 3a), which corresponds to the cloud band. Surface wind vectors shows that southwesterly wind blowing from the land to the sea. The offshore southwesterly wind makes a convergence zone with the westerly wind. This results in the updraft zone along the cloud band. The updraft is intensified just before the landing. Surface precipitation rates of snow and graupel are shown in Fig. 3b. The maximum precipitation rate of graupel is located just behind of the intensified updraft maximum. The maximum of snow precipitation rate is located more inland than that of graupel. Frequent intensifications of the cloud band near the coast would result in a lot of precipitation along the cloud band, and graupel would account relatively large amount in the coastal region.

4. Summary

An observation of snow clouds were performed in Hokuriku, Japan from December 2008 to March 2009, using a polarimetric radar of Nagoya University. Daily numerical simulation

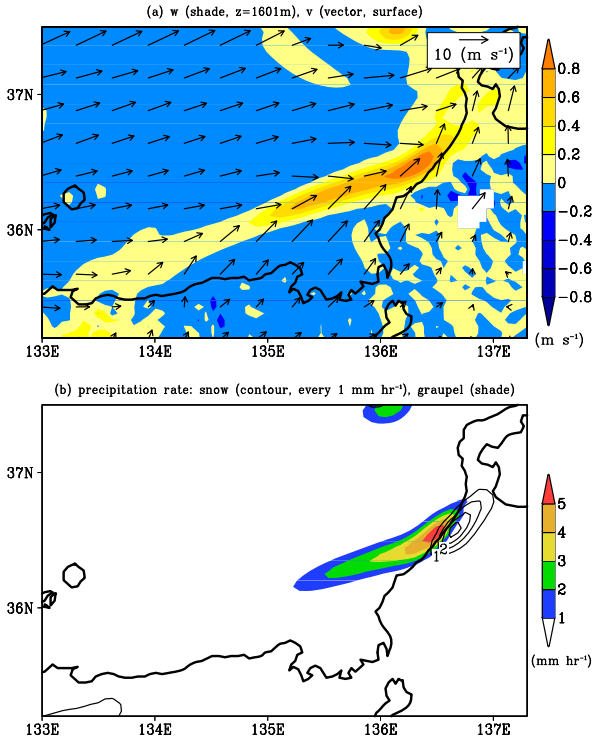

Fig. 3 (a) Vertical velocity (shade, m s^{-1}) at a height of 1601 m and surface horizontal velocity (arrows, m s^{-1}), and (b) precipitation rates (mm hr^{-1}) of snow (contours, every 1 mm hr^{-1}) and graupel (shade) in the simulation results. The corresponding time is 21 JST, 25 January 2009.

experiments were simultaneously performed using CReSS with a horizontal grid spacing of 5 km.

From 00 JST, 25 to 09 JST 27 January 2007, a broad cloud band stayed in the southwest Sea of Japan near the landing part. The landing part of the broad cloud band was intensified. In the CReSS simulation, the updraft along the cloud band forms between southwesterly offshore wind and westerly wind to the north of cloud band, and is intensified near the landing part. The corresponding precipitation at the surface shows graupel accounts relatively large amount in the coastal region.

In the intensified precipitation region around the landing part, examination of polarimetric parameters' distribution would provide useful information associated with distributions of snow and graupel. This is left as a future work.

Acknowledgments

This work was partly supported by Grant-in-Aid for Young Scientists (B) 20740271.

References

Tsuboki, K. and A. Sakakibara, 2002: Large-scale parallel computing of cloud resolving storm simulator. *High Performance Computing* (eds. H. Zima et al.). Springer-Verlag, Berlin-Heidelberg,, 243–259.

Vertical structures of storm: Clues of microphysical processes and density of snow

GyuWon Lee[1], Isztar Zawadzki[2], Andrew Heymsfield[3], David Hudak[4]
Eunsil Jung[3], Peter Rodriguez[4], Frederic Fabry[3], Aaron Bansemer[2], Brian Sheppard[4]

[1]Department of Astronomy and Atmospheric Sciences, Kyungpook National University, Daegu, Korea (ROK)

[2]Department of Atmospheric and Oceanic Sciences, McGill University, Montreal, QC, CANADA

[3]National Center for Atmospheric Research, Boulder, CO, USA

[4]Environment Canada, Toronto, ON, CANADA

The vertical structures of radar reflectivity and radial velocity are a key component to understand the microphysical processes. A classical identification of stratiform and convective rain using the existence of radar bright band is a prominent example. Radar reflectivity provides a general idea on change of mass due to various microphysical processes and existence of melting process. In addition to radar reflectivity, radial velocity information at vertical incidence makes possible to calculate mass flux and a clue of density of snow. For example, snow aggregates have a typical velocity less than 1~2 m/s while rimed snow particles in particular graupel can have velocity larger than a few m/s. The effective density of snow aggregate is typically lower than that of rimed particles. This density difference provides very interesting characteristics of vertical structures of radar reflectivity, radial velocity, and Doppler spectrum.

In the equation of motion, the density or mass of snow is an important factor in change of fall velocity. Particles of high effective density can have fall velocity larger than that of low density. Thus, heavily rimed particles should have fall velocity larger than 1~2 m/s. When the melting process exists, this difference in density also appears in the characteristics of radar bright band. Strong aggregation leads to rapid increase of radar reflectivity while it melts. On the other hand, a rapid increase of radar reflectivity is not expected in bright band for heavy riming. In this paper, we will show the connection among intensity of bright band, microphysical processes, density of snow, and vertical structures of snow.

The use of vertical pointing radar for the study of microphysics has a long history. Recently, the vertical pointing radar can provide Doppler radial velocity and power spectrum in addition to radar reflectivity. These abundant information opens a possibility for more thorough studies of microphysical processes.

McGill University, Canada has been operating a vertically pointing x-band Doppler radar with disdrometers for several years in the Montreal area. This technology was transferred to Kyungpook National University, Korea (ROK). This radar is widely used for microphysical analyses during the summer and winter. We will show some interesting microphysical processes and vertical structures of storm. In addition, the variability of drop size distribution (DSDs) is tackled in terms of microphysics. The variability of DSDs is explained by the quasi-stochastic drop growth equation.

The density of snow is critical information to understand microphysical processes and to improve the accuracy of radar quantitative precipitation estimation (QPE) since it affects radar reflectivity and snowfall rate. A few methods were applied to derive the (effective) density of snow particle as a function of particle diameter. A precise measurement of snow size distribution and fall velocity is essential to solve radar QPE in snow. An extensive observation of snow was performed during the winter of 2005/06 and 2006/07 as a part of Canadian CloudSat/CALIPSO Validation Project. We show microphysical analysis from the various ground-based instrumentations: Hydrometeor Velocity and Size Detector (HVSD), Vertically pointing X-band radar (VertiX), Precipitation Occurrence Sensor System (POSS), C-band dual-polarization, etc.

The effective density of individual snow particle is derived from the equation of motion using the shape and terminal fall velocity of snow particle. The shape and velocity are obtained by HVSD for each particle. This method is verified by comparing the calculated radar reflectivity from HVSD and measured radar reflectivity from VertiX. Results show the significant variation of effective density- diameter relationship from storm to storm and within a storm. Microphysical processes are one of factors that control this variation which is linked with vertical structure of radar reflectivity and Doppler velocity measured by VertiX. In addition, we show systematic difference in the snow size distributions and their variation as functions of microphysical processes such as riming and aggregation. This variation is also consistent with conceptual models derived from quasi-stochastic drop growth equation.

Acknowledgement: This study was financially supported by the Construction Technology Innovation Program(08-Tech-Inovation-F01) through the Research Center of Flood Defence Technology for Next Generation in Korea Institute of Construction & Transportation Technology Evaluation and Planning(KICTEP) of Ministry of Land, Transport and Maritime Affairs(MLTM)

Verification of solid hydrometeor properties simulated by a cloud resolving model using passive microwave radiometer and radar observations

Hisaki Eito and Kazumasa Aonashi

Meteorological Research Institute, Japan Meteorological Agency, Tsukuba, Japan

1. Introduction

Cloud resolving models (CRMs) with complicated cloud microphysical parameterizations explicitly predict various hydrometeors at high time and space resolution; therefore, CRMs serve as valuable tools for satellite remote sensing of precipitation for inferring information about precipitating clouds that cannot be directly observed. However, cloud microphysical validation of CRMs has not sufficiently been carried out. In this study, a CRM, the Japan Meteorological Agency (JMA) nonhydrostatic mesoscale model (JMA-NHM, Saito et al. 2006) is used to simulate typical moderate rainbands associated with the Baiu front observed around the Okinawa Islands, Japan on 8 June 2004. Microwave brightness temperatures (TBs) and equivalent radar reflectivities are derived from the model output, and are then compared to concurrent corresponding satellite radiometer (AMSR-E, Kawanishi et al. 2003) and ground-based radar (COBRA, Nakagawa et al. 2003) observations. The objectives of this study are to verify the two-moment bulk microphysics of the JMA-NHM and to examine some of the microphysical sensitivities. Special attention is given to the characteristics and sensitivities of frozen hydrometeor properties simulated by the JMA-NHM.

2. Models

The JMA-NHM is an operational nonhydrostatic mesoscale model developed by the JMA. Observed rainbands are simulated with one-way double-nested domains having horizontal grid sizes of 5 and 2 km. The same physical parameterization is used for the double-nested domains, except that the Kain-Fritcsh convective parameterization scheme is not used in the inner domain. An explicit three-ice bulk microphysics scheme (Ikawa and Saito 1991) is incorporated. This scheme predicts the mixing ratios of six water species (water vapor, cloud water, rain, cloud ice, snow and graupel) and number concentrations of ice particles. The size distributions for each precipitation particles are represented by exponential functions.

The radiative transfer model (RTM) developed by Liu (1998), which uses plane-parallel and spherical particle approximations, is used to simulate TBs in this study. TBs are obtained for each grid using the RTM interfaced with the JMA-NHM simulations. The simulated TBs are convolved with a Gaussian function that is close to the actual AMSR-E antenna patterns for each frequency, and then compared to concurrent corresponding AMSR-E observations.

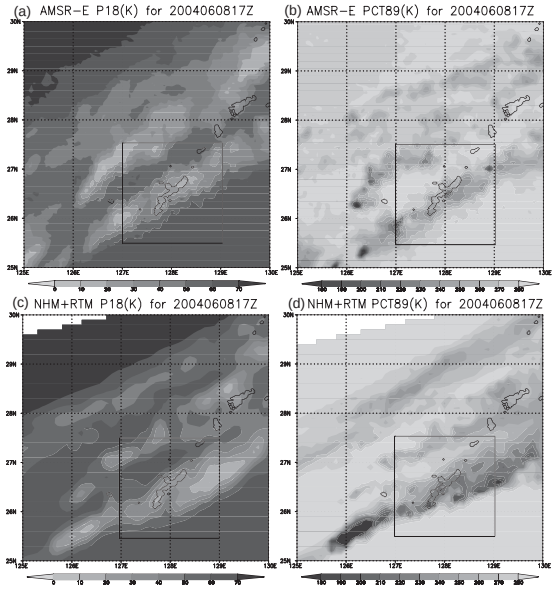

Fig. 1. (a) P18 and (b) PCT89 retrieved from TBs observed by AMSR-E at 17 UTC on 8 June 2004. (c) P18 and (d) PCT89 retrieved from TBs simulated by the JMA-NHM at 17 UTC on 8 June 2004. The rectangles represent the location of the area analyzed in Fig. 4.

3. Comparisons of simulations with observations

Figure 1a shows the polarization difference (vertically polarized TB minus horizontally polarized TB) at 18.7 GHz (P18) observed by AMSR-E at 1700 UTC on 8 June 2004. A P18 approaching zero corresponds to increasing absorption by rain and cloud water particles. Areas with low values of P18 are found in the rainbands, indicating the presence of large amounts of liquid water. The polarization-corrected temperatures (PCTs, Spencer et al. 1989) retrieved from the 89.0 GHz TB (PCT89) are presented in Fig. 1b. The depression of PCT89 is caused by scattering by frozen hydrometeors. Areas with depressions in PCT89 are also found in the rainbands, denoting that frozen hydrometeors also exist in those bands. Figures 1c and 1d depict P18 and PCT89 simulated by the JMA-NHM and RTM at 1700 UTC on 8 June 2004. The values of simulated P18 are almost in agreement with those of the AMSR-E observations. However, the simulated PCT89 depression is larger than the observed one. This result suggests that the JMA-NHM adequately simulates the amount of liquid hydrometeors; however, it overestimates the amount of frozen hydrometeors.

The JMA-NHM and COBRA data are compared using a statistical technique, contoured frequency with altitude diagrams (CFADs, Yuter and Houze 1995). Figure 2a depicts the reflectivity CFAD obtained from

the COBRA observations. The highest probabilities follow a coherent pattern with the peak density gradually decreasing with height from between 25 and 35 dBZ near the melting level (about 4.5 km in height) to between 10 and 20 dBZ near the storm top at 13 km. Below the melting level, peak probabilities are almost constant to the surface. Figure 2b depicts the reflectivity CFAD obtained by the JMA-NHM simulation. Overall, good agreement is observed between the observations and the simulation. The highest probabilities also demonstrate a coherent pattern with peak densities similar to those of the observations. Below the melting level, peak probabilities for the simulated reflectivities agree with those from the observation. However, peak probabilities from the simulation appear to shift slightly higher above the melting level. This result suggests that model captures the observed reflectivities in the liquid phase fairly well; however, it slightly overestimates the size of hydrometeors in the ice phase.

The dominant form of ice in the simulation was snow with much smaller amounts of graupel and cloud ice (not shown). It seems reasonable that the dominant form of frozen hydrometeors is snow in this case; however, comparison with radar and radiometer data indicates that the amount of model-simulated snow is probably too large. This was caused by the JMA-NHM overestimation of the amount of snow through depositional growth (not shown).

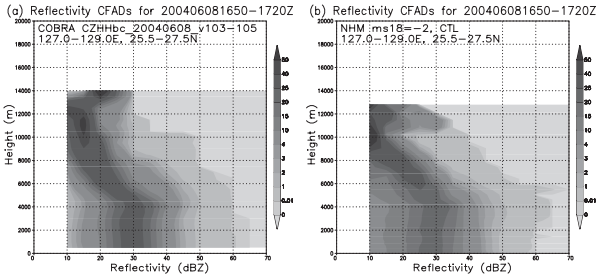

Fig. 2. Reflectivity CFADs for the region of 127–129°E, 25.5–27.5°N and the period from 1650 to 1720 UTC on 8 June 2004 derived from (a) the observed CORBA radar reflectivity data and (b) the JMA-NHM simulation.

4. Sensitivity experiments

As discussed in the previous section, comparisons with radar and radiometer observations suggest that the model overestimates the size and amount of snow. Based on those results, we conduct three sensitivity experiments (experiment IN, experiment PSACW, and experiment FVS) that involve adjustments to the snow microphysical parameters to quantify the process sensitivities in order to reduce excessive snow in the control experiment. In experiment IN, the ice nucleation process is changed to reduce the ice nucleation rate. This change reduces the depositional growth of snow due to a reduction in the number concentration of snow generated by the conversion of cloud ice. In experiment PSACW, the riming threshold for snow to graupel conversion is changed so that almost all of the accreted cloud water is converted into graupel. In experiment FVS, a higher snow fall speed is used so that snow particles quickly sediment out.

The mixing ratios of snow in all the sensitivity experiments are reduced from the control experiment (not shown), indicating that each adjustment has a positive impact in reducing the excessive snow. In experiments PSACW and FVS, the mean diameter is also reduced from the control experiment (not shown), due to the reduction in snow mixing ratios. In contrast, the mean diameter in experiment IN becomes larger than that of the control experiment (not shown), due to the large reduction in snow number concentration.

Profiles of probability density of the observed and simulated radar reflectivities for two levels at heights of 2.0 and 7.0 km are presented in Fig. 3. At a height of 2.0 km (Fig. 3a), under the melting level, the profiles for the sensitivity experiments are similar to those of the control experiment and the radar observations. At a height of 7.0 km (Fig. 3b), above the melting level, the peak probabilities at 20 dBZ in experiments PSACW and FVS shift closer to the observed value. In contrast, the peak probability at 25 dBZ in experiment IN remains similar to that of the control experiment and still shifts higher than the radar value.

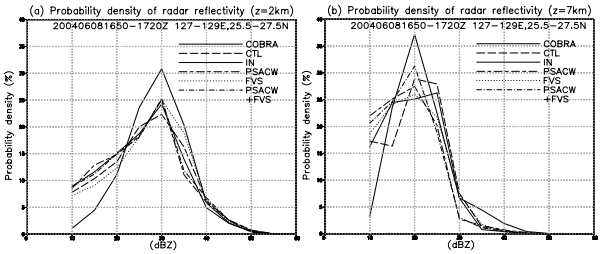

Fig. 3. Probability densities of reflectivity for the region of 127–129°E, 25.5–27.5°N at 1700 UTC on 8 June 2004 at a height of (a) 2 km and (b) 7 km. The probability density derived from the observed CORBA radar reflectivity data is denoted by the solid line, and the JMA-NHM simulations are denoted by the dashed line (the control experiment), thin solid line (experiment IN), short-long dashed line (experiment PSACW), dotted line (experiment FVS), and dot-dashed line (experiment PSACW+FVS).

Profiles of probability densities for P18 and PCT89 are presented in Fig. 4. The profiles of P18 in the sensitivity experiments shift closer to those in the observations (Fig. 4a). As indicated in Fig. 4b, probabilities of PCT89 less than 210 K in experiment

PSACW are slightly smaller than those for the control experiment, indicating that experiment PSACW performs better for reducing the overdepression of PCT89. In experiment FVS, fewer PCT89 values less than 230 K occur than in the control experiment, in better agreement with the observation.

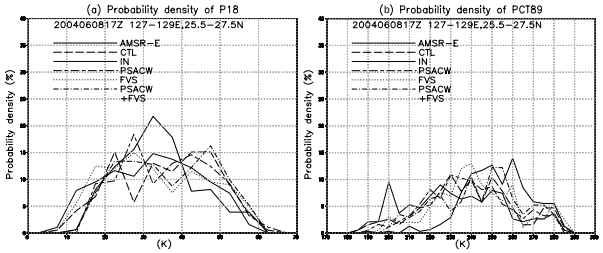

Fig. 4. Probability densities of (a) P18 and (b) PCT89 for the region of 127–129°E, 25.5–27.5°N at 17 UTC on 8 June 2004. Probability densities derived from the observed AMSR-E data are indicated by the solid lines, and the JMA-NHM simulations are denoted by the dashed line (the control experiment), thin solid line (experiment IN), short-long dashed line (experiment PSACW), dotted line (experiment FVS), and dot-dashed line (experiment PSACW+FVS).

Based on these results, an additional experiment is conducted using both adjustments to the microphysical parameters from experiments PSACW and FVS (experiment PSACW+FVS). Experiment PSACW+FVS performs better for reducing the excessive amount and size of snow (not shown). As a result, experiment PSACW+FVS also performs better for reducing overdepression of PCT89 (Fig. 4b). Moreover, above the melting level, reflectivities of 20 dBZ occur more frequently in experiment PSACW+FVS than in the other experiments, in better agreement with the radar observations (Fig. 3b). However, the probabilities of PCT89 less than 230 K even in experiment PSACW+FVS remain greater than were observed. These results suggest that the amount of snow is still excessive and that further adjustment to and improvement of the snow microphysical processes are necessary.

5. Summary

TBs and reflectivities simulations were conducted for rainbands around Okinawa Islands, Japan, which were compared to the timely corresponding AMSR-E and COBRA observations. Fairly good agreement was obtained between the simulation and observations in liquid phase, indicating that the JMA-NHM adequately simulated the amount of liquid hydrometeors. The intensity of scattering in the simulations was stronger than that in the observations above the melting layer, due to the fact that the JMA-NHM overestimated the amount and size of snow particles as a result of large depositional growth. The excessive snow contents were reduced by adjusting some of the microphysical processes in the JMA-NHM: the snowfall speeds were increased and a riming threshold for snow to graupel conversion was changed.

More analyses of many more situations and events are needed to estimate the generality of the model verification and microphysical sensitivities of the JMA-NHM presented in this study.

Acknowledgements

The authors express their thanks to Koyuru Iwanami of the National Research Institute for Earth Science and Disaster Prevention and Katsuhiro Nakagawa, Hiroshi Hanado, Yasushi Kitamura and Yukari Shusse of the National Institute of Information and Communications Technology for supplying the COBRA data. This study was partially supported by the Japan Aerospace Exploration Agency. The numerical experiments were performed using the SX-6 computer at the Meteorological Research Institute.

References

Ikawa, M. and K. Saito, 1991: Description of a nonhydrostatic model developed at the Forecast Research Department of the MRI. *Tech. Rep. MRI*, **28**, 238 pp.

Kawanishi, T., and Coauthors, 2003: The Advanced Microwave Scanning Radiometer for the Earth Observing System (AMSR-E), NASDA's contribution to the EOS for global energy and water cycle studies. *IEEE Trans. Geosci. Remote Sens.*, **41**, 184–194.

Liu G. 1998: A fast and accurate model for microwave radiance calculations. *J. Meteor. Soc. Japan*, **76**, 335–343.

Nakagawa, K., and Coauthors, 2003: Development of a new C-band polarimetric Doppler weather radar in Japan. *Proc. 23rd IGARSS*, 4462–4464.

Saito, K., and Coauthors, 2006 : The operational JMA nonhydrostatic model. *Mon. Wea. Rev.*, **134**, 1266–1298.

Spencer, R. W., H. M. Goodman, and R. E. Hood, 1989: Precipitation retrieval over land and ocean with the SSM/I: Identification and characteristics of the scattering signal. *J. Atmos. Ocean. Tech.*, **6**, 254–273.

Yuter, S. E. and R. A. Houze Jr., 1995: Three-dimensional kinematic and microphysical evolution of Florida cumulonimbus. Part II: Frequency distributions of vertical velocity, reflectivity, and differential reflectivity. *Mon. Wea. Rev.*, **123**, 1941–1963.